CHAPTER IV
RESULTS AND DISCUSSION

Sintering of a mixture of Mn and Bi powders is adopted for synthesizing LTP-MnBi due to its possibility for scaling up in production. To greatly reduce post-processing steps such grinding and low-temperature annealing, sintering was performed at temperatures just above melting point of Bi and low enough that high-temperature phase MnBi was not formed. This low temperature allows sintering to be in liquid phase, i.e., liquid-phase sintering (LPS). One more important consideration in designing the conditions for LPS is that the process must be taken place in an absence of oxygen to avoid formation of Mn oxides. It is noted again that the sintering was performed at vacuum pressure below 5×10^{-7} mbar.

The first two sections of this chapter report the phases, morphology, elemental composition, and magnetic properties of the sintered product. More importantly, the mechanism for the formation of LTP-MnBi during LPS is also explained. Two set of samples were investigated. The first set of samples was sintered at 275 °C, 325 °C and 375 °C for 12 hr. The second set sintered at 325 °C with different durations of 12, 24, and 48 hr, respectively.

The stability of magnetic properties is also essential when magnetic materials will be used in devices. It is known that the magnetic properties of LTP-MnBi could be affected by different factors such as crystal structure, and microstructure as oxidation (Janotová, Švec, Maťko, Janičkovič and Sr., 2018; Ly et al., 2014; Villanueva et al., 2019) that could be altered by decomposition (Ly et al., 2014; Sun, Xu, Liang, Sun and Zheng, 2016) by exposure to humidity (Jacobson and Kim, 1987) and elevated temperature (S. Cao et al., 2011; Chen et al., 2015; J. Cui et al., 2014; D. T. Zhang et al., 2014) for an extended period of time. The studies of long-term stability of LTP- MnBi are reported in the third section of this chapter. The last section of this chapter covers the investigation of the decomposition of LTP- MnBi at 150 °C.

4.1 LTP-MnBi sintered at 275, 325 and 375 °C for 12 hours

4.1.1 Phase identification

After sintering, the sintered product was a rod with the inner shape of the quartz tube used in the effusion cell. The sintered product was ground and sieved into 2 sets of MnBi powder sizes, i.e., less than <20 μm defined as the small particle size and large particle size is defined for the 20-53 μm size. It is noted that the initial size of Mn was less than 20 μm prior to sintering. Thus, the large particles were resulted from agglomerations of smaller particles. The MnBi powders were characterized to study crystal structure by the X-ray diffraction technique (XRD) using a Bruker D2 phaser X-ray diffractometer. Figure 4.1 shows the XRD patterns taken from all sintered MnBi samples. The Bi phase (card No. 96-231-0890), MnBi phases (card No. 96-900-8900), and MnO phases (card No. 96-101-0394) were identified, appearing as diffraction peaks in the figure. However, Mn phase could not be detected due to the limit of X-ray penetration depth (P.-K. Nguyen, Jin and Berkowitz, 2013). The unreacted Mn was expected to be remain in the Mn powder particle under the forming MnBi layer. The thickness of the newly formed MnBi layer is thicker than the X-ray penetration depth, preventing the unreacted Mn in the powder particles to be detected. In addition, there is Bi covering on the particles, and thus the Bi further reduce the chance for X-ray to detect the Mn phase in this sintered product.

The obtained XRD patterns were analyzed to determine the crystallization quality. The crystallization quality could be calculated from the average full width at half maximum (FWHM), the first four main MnBi peaks i.e. (101), (002), (012) and (110) planes peaks were selected. The FWHM values of MnBi-275, MnBi-325 and MnBi-375 were 0.176, 0.194, and 0.214 degrees, for the small particle size and 0.164, 0.170, and 0.169 deg for the large particle size. Next, the crystallite size could be estimated from the Scherrer equation, that is $D = \frac{K\lambda}{BCOS\theta}$, where K = 0.9 is the shape factor constant. The crystallite size values of 51.4, 45.9 and 41.2 nm for the small particle size and 55.0, 52.1 and 53.3 nm for the large particle size, respectively. It is obvious that these values of all samples have similar values in range of 41-55 nm.

For more detailed analysis, the different phase contents for the small and large samples were estimated by using the Rietveld refinement method of XRD data using the FULLPROF program. The MnBi phase contents were found to be 56.1, 59.5, 52.8 wt% for the small particle size and 69.3, 70.1, 66 wt.% for the large particle size with sintering temperature at 275 °C, 325 °C and 375 °C, respectively. For both sample sizes, it is indicated that the MnBi content increased with sintering temperature from 275 °C to 325 °C and decreasing at 375 °C. The slight increase in MnBi content when sintering temperature increase from 275 °C to 325 °C may be due to the increase in the diffusion rate with temperature. A significant reduction in MnBi content of the MnBi sintered at 375 °C could be explained by the Mn-Bi segregation during LTP- to HTP-MnBi phase transition at temperature above 350 °C (Jun Cui et al., 2018). Due to the shallow X-ray penetration depth, Mn cores could not be detected, the content values reported here does not represent the exact MnBi ratio. One more interesting point obvious in the XRD pattern is that more Bi was observed in the smaller samples. This might be due to the fact that the unreacted Bi in the sintered product could easily be ground to powder with particle sizes smaller than 20 μm.

It is interesting to point out that MnO was also observed in the XRD patterns. The amount of the oxide was estimated to be less than a few wt.% for all samples. The base pressure of the sintering system was about 2×10^{-8} mbar, and the vacuum pressure during sintering process was controlled to be below 5×10^{-7} mbar, which is the upper limit pressure for filaments of the effusion. It is understood that at the sintering temperatures used in this work, Mn powder particles were coated or immersed in liquid Bi. More importantly, there is no significant difference in the amount of the oxide formed on the samples sintered at the three different temperatures. Oxidation rate is generally known to increase with temperature. Thus, oxide formation during sintering must be very low and below our detection limit. However, it was observed that the amount of the oxide increased with time after the sintered MnBi was exposed air. The formation of oxide at this stage might be considered as the degradation as there has been a report earlier (Janotová et al., 2018).

It is worth to emphasize that the single-step vacuum sintering method can be considered as a facile MnBi preparation method. Moreover, the purity of MnBi can be further enhanced by using magnetic separation (S. Kim et al. 2017), optimizing the Mn content (B.A. Jensen et al., 2019) or, in principle, reducing the starting Mn particle size.

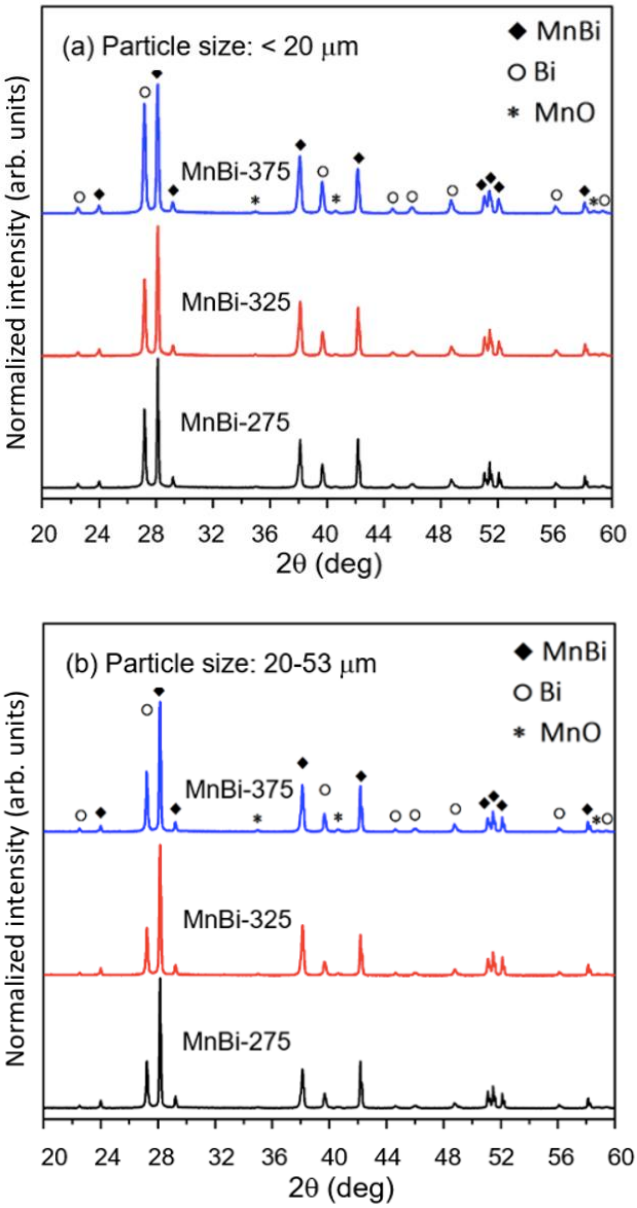

Figure 4.1 XRD patterns of LTP-MnBi powder prepared at various annealing temperature at 275 °C, 325 °C and 375 °C for small particle size of (a) < 20 μm and (b) 20-53 μm.

4.1.2 Morphology and size distribution

Figure 4.2(a) and (b) show SEM images of the MnBi-275 powder particles for two different size ranges illustrating their typical morphologies. The starting material of Mn powder particles was prepared to be less than 20 μm in size, and the individual Mn particles shall still be less than 20 μm in size because the sintering temperature is below the melting point of Mn. Thus, there is virtually no changes in particle size for Mn before and after sintering. The formation of MnBi is assumed to be mainly controlled by diffusion mechanism of the melted Bi. The single MnBi particle size was measured to be about 8 μm, as seen in Figure 4.2(a). It is obvious that the larger particle size is likely an agglomeration of several MnBi particles, bonded with Bi, with a total size of around 29 μm, as shown in Figure 4.2(b).

The elemental composition of the sintered product was investigated by the SEM/ EDS technique. EDS measurements of the MnBi powder particle sample, shown in Figure 4.2(a) were performed at three specific points. Since this technique cannot probe very deep into the bulk. The composition reported here is mainly surface composition. It was observed that the surface composition of the selected particle varies from position to position, as indicated by the white (point A and B) and grey (point C) areas. The calculated Bi/Mn content ratios are given in the inset of Figure 4.2(a). It was found that there are two main distinguished areas two different ratios; those are the MnBi rich area with Bi/Mn ratio ~ 1 and the Bi-rich area with Bi/Mn ratio >>1. It is noted that the area Mn-rich area (Bi/Mn ratio <<1) was not observed.

From the analysis of SEM images and EDS spectra, the whole MnBi formation process can be explained as follows. At a sintering temperature higher than the Bi melting point, Bi is melted to be liquid migrating over the surfaces of Mn power particles. It is expected that the Mn powder particles were covered by liquid Bi. At the interface between solid Mn and liquid Bi, there is the chemical interactions between Bi and Mn to form an MnBi layer. The thickness of the MnBi layer is increased by diffusion of Mn and/or Bi across the forming MnBi layer. Since the atomic ratio of 1:1 for the starting Mn and Bi powder was used in

the sample preparation, the single-phase MnBi could be expected in the completed sintering process.

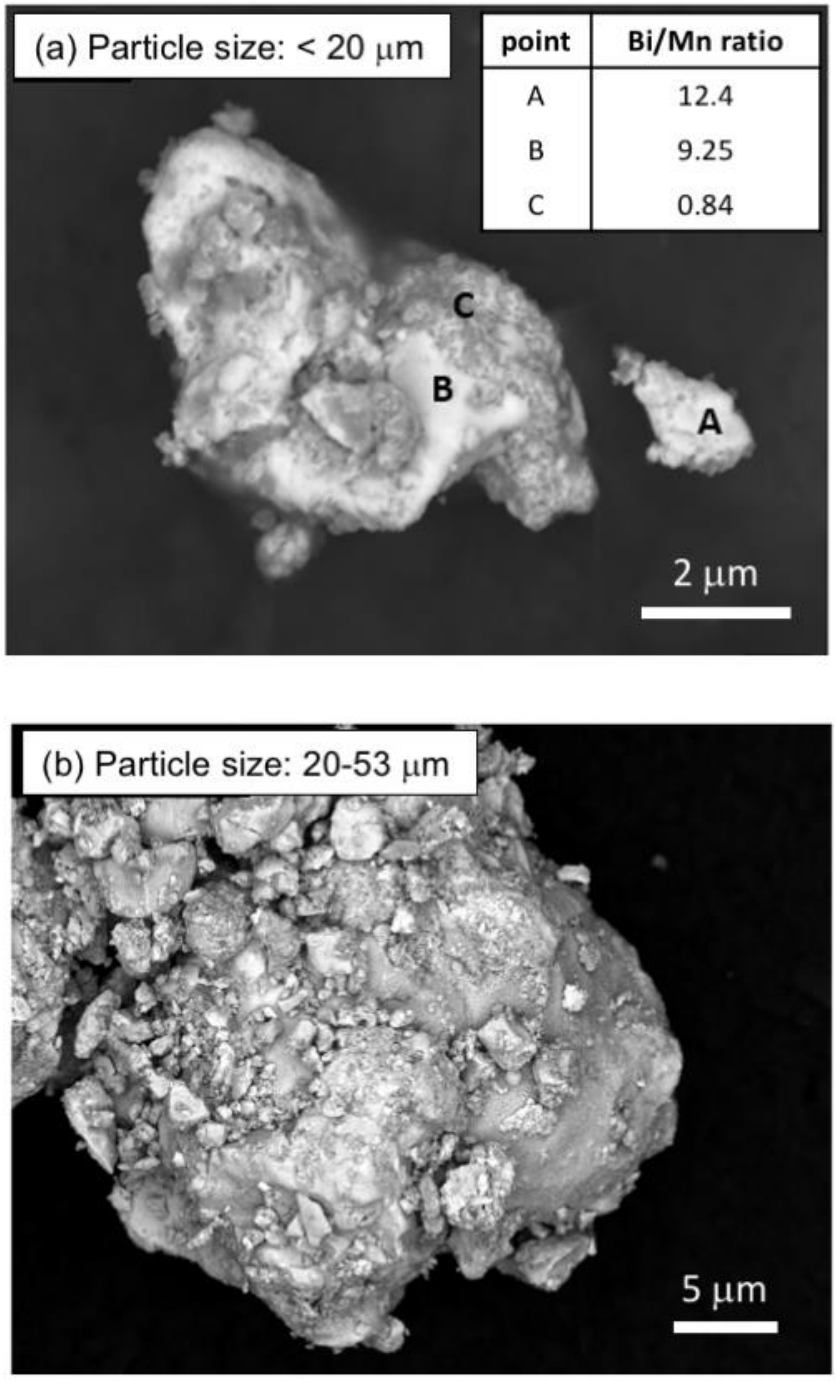

Figure 4.2 SEM images of the MnBi samples sintered at 275 °C with particle sizes of (a) < 20 μm and (b) 20-53 μm. The inset in (a) is the Bi/Mn ratio obtained from the EDS analysis of three specific locations.

However, because the starting Mn powder particle is large, the formation of the MnBi layer is, thus, limited by the diffusion mechanism. The evidence of an incomplete process can be observed by the excessively Bi-rich areas (points A and B of Figure 4.2(a)) and the Bi phase detected from XRD results. From above arguments, it is expected that unreacted Mn shall remain in the sintered product even though this unreacted Mn could not be detected by the XRD and SEM/EDS measurements. Cross-sectional MnBi powder particle sample for EDS measurement was required to identify this assumption, which are to be shown below.

4.1.3 Magnetic properties

Figure 4.3(a) and (b) show the experimental room-temperature M-H curves with a demagnetizing field correction for the small and large MnBi particle sizes, respectively. The inset of Figure 4.3(a) shows the demagnetization curves of raw *M (N = 0),* corrected *M (N = 0.4)*, corrected *B (N = 0.4)* and the $(BH)_{max}$ area (dashed rectangle) of the small MnBi particle size sample. Demagnetizing field correction is necessary for analysis of the M-H curves taken from strong magnetic materials because VSM measurements are open-loop measurements. The corrected magnetic field is $H_{int} = H_{applied} - 4\pi N_D M$, where N_D is the sample demagnetization factor (SI units) and M is the volume magnetization in emu/cm^3. This H_{int} parameter can be calculated the magnetic induction equation is created from $B = H_{int} + 4\pi M = H_{applied} + 4\pi M(1-N_D)$. The area of the largest square in the second quadrant multiplied by the value of point *B* and *H* is the maximum energy produce. The square loop with a demagnetizing field correction is improved while the value of H_{ci} and M_s has not changed. It is noted that the measured samples were in the powder form, not in a compressed bulk, composing of Mn particles with LTP-MnBi surface layer and Bi.

The values of weight percentage of MnBi content and important magnetic properties of all sintered MnBi samples are given in Table 4.1. The small particle sizes samples sintered at 275 °C, 325 °C and 375 °C have the intrinsic coercivities (H_{ci}) of 4.88$\pm$ 0.24, 4.98 $\pm$ 0.24 and 6.0 $\pm$ 0.30 kOe, and the saturation magnetizations (M_s) of 44.99 $\pm$ 2.25, 45.79 $\pm$ 2.29 and 39.61 $\pm$ 1.98 emu/g, respectively.

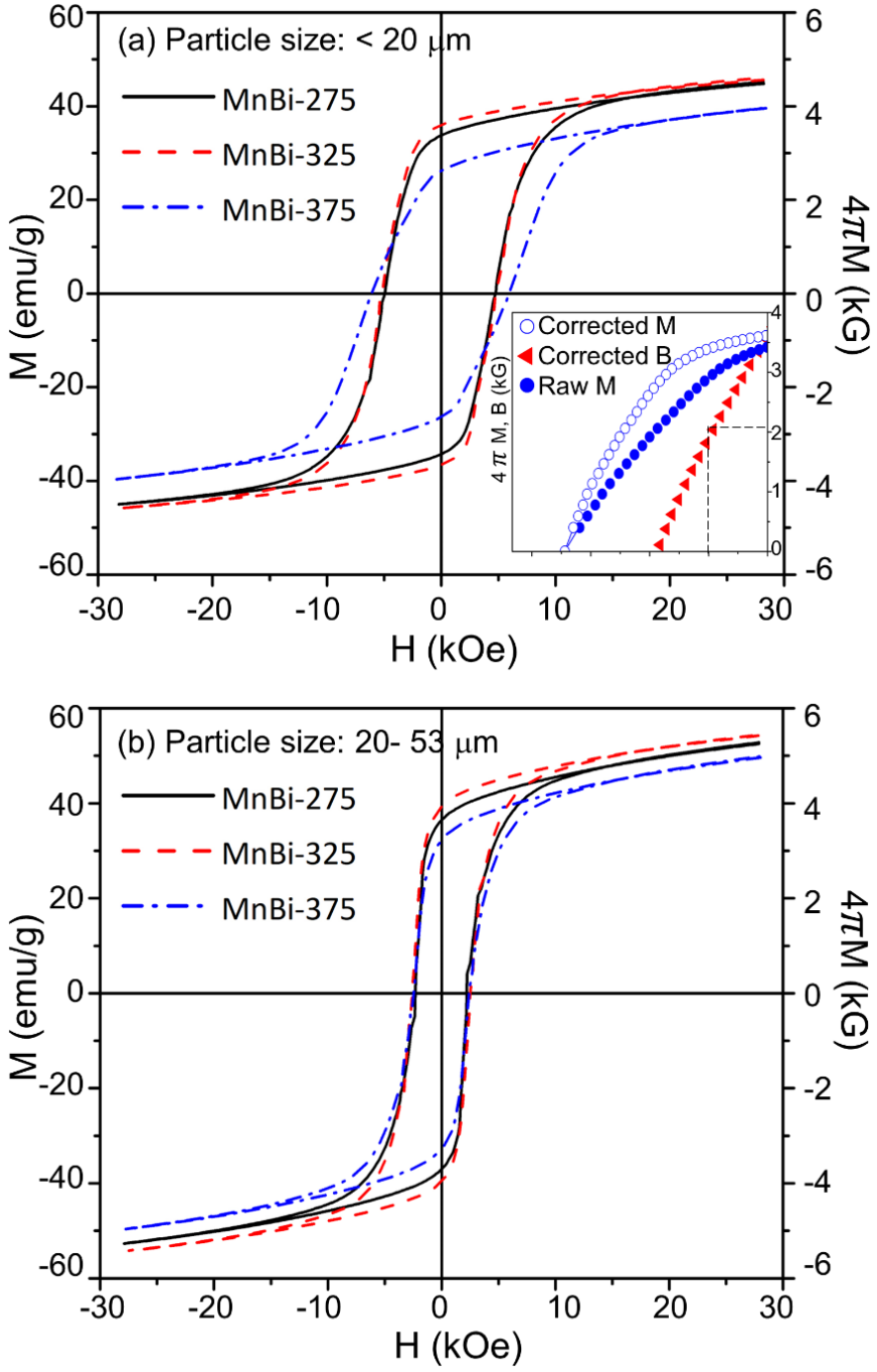

Figure 4.3 The M-H curves with demagnetizing field correction of the MnBi samples sintered at 275, 325 and 375 °C for particle sizes of (a) < 20 μm and (b) 20-53 μm. The inset in (a) shows the demagnetization curves of raw M (N = 0), corrected M (N = 0.4), corrected B (N = 0.4) of the small MnBi sintered at 325 °C. The $(BH)_{max}$ is the dashed rectangle with maximum area.

The M-H curve of the small MnBi size sample sintered at 325 °C shows better performance magnetic properties than the small MnBi sample sintered at 275 °C. This may be explained by a higher formation rate of MnBi layer at higher sintering temperature, leading to high LTP-MnBi content in the sintered product. It is important to note that the shape of M-H curve for small size MnBi sample sintered at 375 °C is different from those sintered at lower temperatures. The value of H_{ci} increases but the M_s decreases. The M_s is related to MnBi content, therefore it is suggested that sintering at 375 °C might cause the formation of HTP-MnBi. The formation of HTP-MnBi consequently is affected to achieve the low MnBi content. This observation from VSM is similar what have been observed in the XRD patterns reported above.

Table 4.1 The weight percentage of MnBi content and magnetic behaviors of all sintered MnBi sample.

Sample ID	MnBi (wt.%)	M_s (emu/g)	H_{ci} (kOe)	$(BH)_{max}$ (MGOe)
small MnBi-275	56.1	44.99 ± 2.25	4.88 ± 0.24	2.46
small MnBi-325	59.5	45.79 ± 2.29	4.98 ± 0.24	2.84
small MnBi-375	52.8	39.61 ± 1.98	6.00 ± 0.30	1.48
big MnBi-275	69.3	52.64 ± 2.63	2.09 ± 0.12	2.33
big MnBi-325	70.1	54.27 ± 2.73	2.49 ± 0.10	2.63
big MnBi-375	66.0	49.71 ± 2.48	2.54 ± 0.14	1.78

From the data presented in Table 4.1, it is obvious that the small particle size MnBi sample exhibits higher H_{ci} but slightly lower M_s, which is agreed with other reports (J. Cao et al., 2019; X. Li, Pan, Zhen, Lu and Batalu, 2019). The H_{ci} of small MnBi particle is approximately higher 2 times than that of the large one. The higher H_{ci} observed in

smaller particles could result from the refinement of MnBi grains, leading to more uniform rotation of magnetic moments (B. Li et al., 2018; Y. Zhang et al., 2017). There has been a report of the theoretical saturated magnetization of for LTP-MnBi, which was calculated to be 80 emu/g at room temperature (Sarkar and Basu Mallick, 2020). This theoretical value of the saturated magnetization may be used to estimate the LTP-MnBi fraction or content, assuming a linear relation between the fraction and the saturated magnetization. For the small and large particle size samples sintered at 275 °C, the LTP-MnBi was found to be 56% and 65.6%, respectively. The results deduced from VSM measurements are consistent with the XRD results showing that patterns for smaller particle sizes contain higher diffraction intensity peaks from elemental Bi. There has been also a report showing that the decrease in magnetization could be (Kharel et al., 2013). It is apparent that samples with diverged particle sizes have a similar tendency of $(BH)_{max}$ with varied sintering temperature. The highest $(BH)_{max}$ of 2.84 MGOe was obtained in the small MnBi sample sintered at 325 °C. The magnetic properties of all MnBi powders are summarized in Table 4.1.

Figure 4.4 shows the M-H curves of fresh and 10-month-old MnBi-275 measured at different sample temperatures. These MnBi sample was sintered at 275 °C for 12 hours. There is an obvious difference in the M-H curves for the fresh and old sample. The old sample exhibits the degradation since the sample was left in air for extended time (M. Y. Sun et al., 2016) which is the topic for the last section of this chapter. The interesting result is the measurement results taken from the 10-month-old sample at different sample temperatures, i.e., 300K, 350K and 400K. There are continuous changes in shape of the M-H curve when the temperature increases from 300K to 400K. The M_s decreases while the H_c increase with the sample temperature which is similar to what have been observed with MnBi prepared by different techniques (J. Cao et al., 2019; Chen et al., 2016; J. Cui et al., 2014). It is noted that the kinks of magnetization curve are larger at higher measuring temperature, which created from the weakened coupling between different magnetic phases such as MnBi, Mn, Bi and amorphous (Xie et al., 2016; Yang et al., 2014), including to the possible formation of new phases at elevated temperature during the VSM measurements.

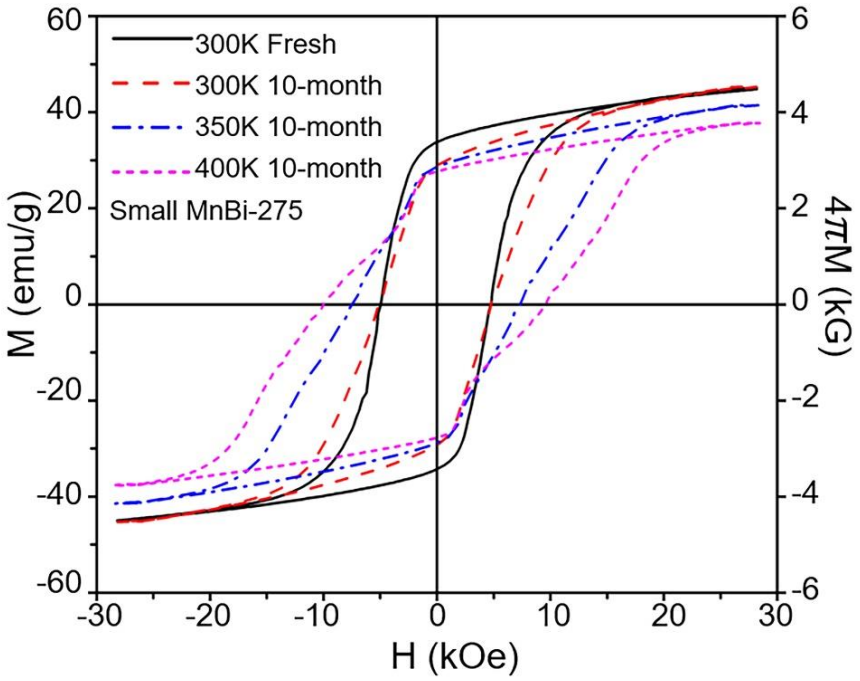

Figure 4.4 M-H curves measured at sample temperature of 300K, 350K and 400K for the fresh and 10-month-old MnBi samples sintered at 275 ºC showing the increase of coercivity with temperature.

4.1.4 Depth profile and diffusion in MnBi layers

Huge efforts have been spent in preparing cross-sectional powder particles for SEM/EDS measurements for investigation of elemental depth profile and diffusion of Bi and Mn in MnBi layer. A cross-sectional SEM micrograph of an as-received Mn powder particle with size of about 100 μm is shown in Figure 4.5(a). Even without any sample treatments, there many cracks in the Mn powder particle as shown in the figure. For this study, this as-received Mn powder was mixed with Bi powder and then sintered at temperatures in the vicinity of liquid-phase sintering (LPS), in which Mn remains solid while the Bi transforms to liquid. It was expected that, upon LPS, Bi transforms to liquid covering the Mn powder particles. Some Bi flows into the cracks in the Mn particles. Bi atoms interact with Mn atoms at the surface of the particle and at both surfaces of the cracks. LTP-MnBi formed at the external surface of Mn particles and the interior-surfaces along the cracks.

After sintering process, the cross-sectional SEM for MnBi powder particles sintered at 275 °C, 325 °C and 375 °C which are shown in Figure 4.5(b), (c) and (d), respectively. All-sintered cross-section MnBi samples show a spider-web feature composite of white areas (Bi rich), and gray areas (Mn rich) in the Mn particles. The white areas appear near the cracks and the external surface of Mn particles, and these areas is expected to be LTP-MnBi layers formed during. At melting point of Bi, Bi transformed to liquid Bi while Mn remains solid. Bi interact with Mn to form MnBi layer at the external surface of Mn particles and the interior-surfaces along the cracks.

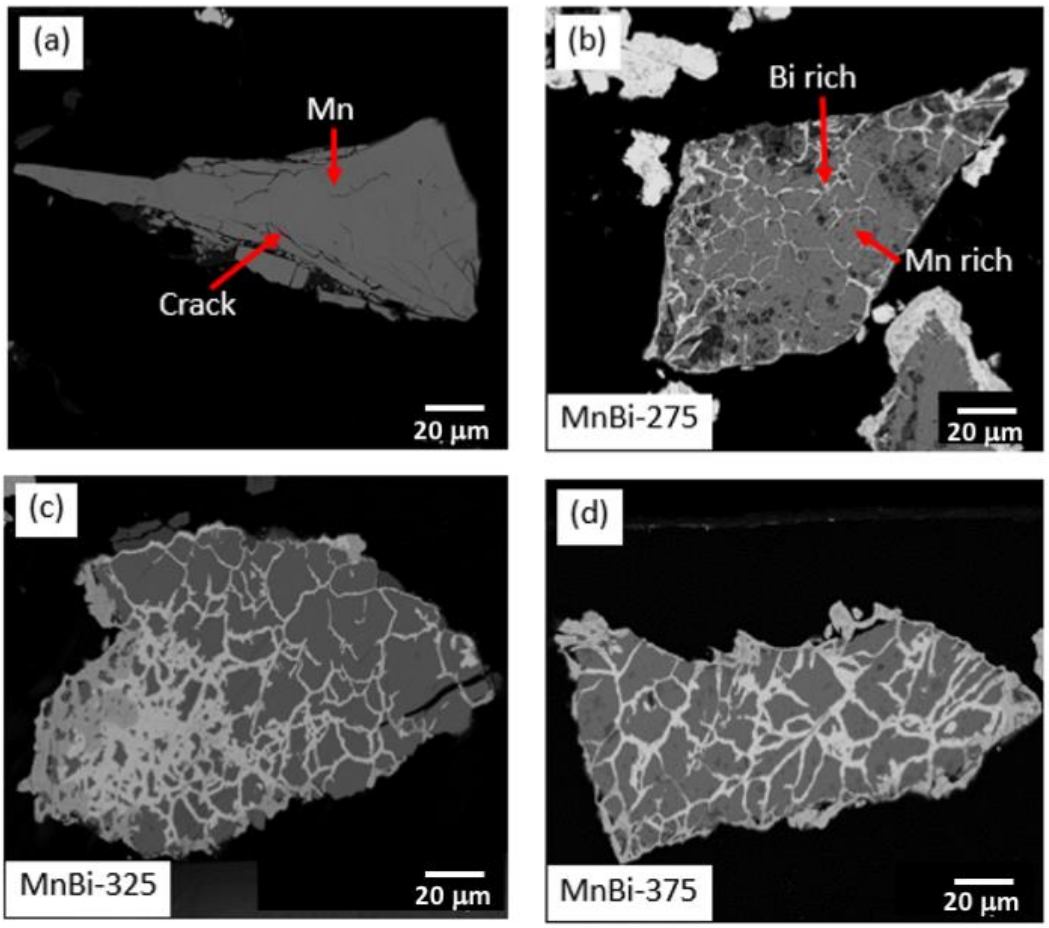

Figure 4.5 The cross-sectional SEM images of (a) as-received Mn powder particle (b) Mn powder particles sintered at 275 °C (c) at 325 °C and (d) at 375 °C.

Figure 4.6(a) shows the typical zoom-in cross-sectional SEM micrograph near the crack in MnBi particle sample sintered at 325 °C, which appears as a vertical grey line in the middle of the figure. The formation of MnBi layers occurred at both side-surfaces of the crack and extended deep into the bulk. This results in the formation of MnBi layers along crack surfaces, which appear as the bright stripes along both sides of the crack in the SEM image. Further from cracks, only unreacted bulk Mn is observed: the grey areas on both sides. The observed thicknesses of the MnBi stripes formed on opposite sides of a crack are different. There is no symmetry reason for the MnBi layers formed on opposite banks of the Bi river to grow at precisely the same rate. The difference may be dominated from the effect of sample preparation being conducted at an angle to the crack as shown in the inset of Figure. 4.6(a).

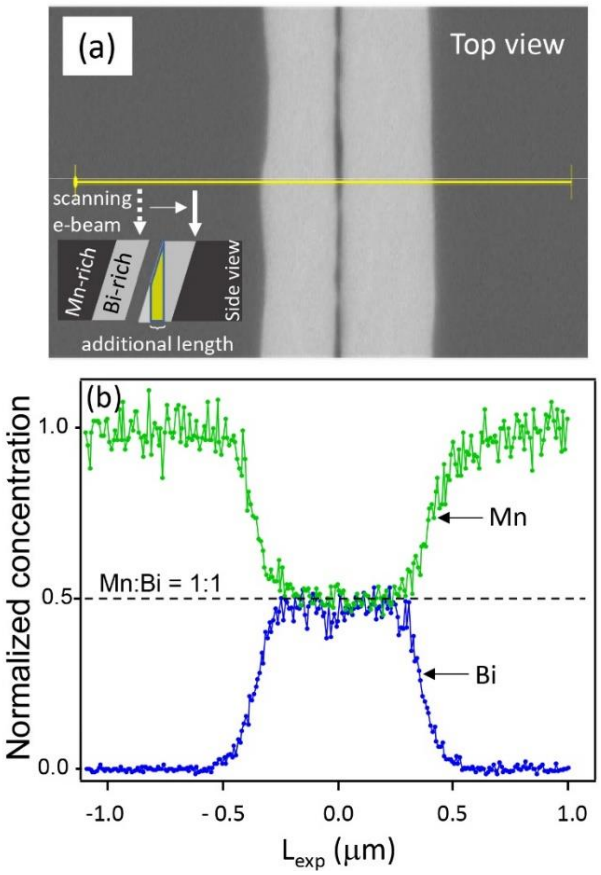

Figure 4.6 (a) Zoom-in cross-sectional SEM image of the MnBi sintered at 325 °C. Inset illustrates the side-view schematic which may yield to different forming thickness between each side of the crack. (b) The Bi and Mn concentration profiles along the yellow line of (a).

The elemental depth profiles of the MnBi layers were obtained from EDS line scans along the yellow line in Figure. 4.6(a)The Mn and Bi depth profiles taken from the MnBi sample sintered at 325 °C are shown in Figure. 4.6(b). They indicated that the sintered MnBi layers are composed of homogenous and graded regions. Near the surface of the cracks, homogenous MnBi regions formed with Mn and Bi in an atomic ratio of 1:1. Beyond this homogenous region, the concentration of Bi decreases with depth. For this EDS line scan shown in Figure. 4.6(b), the Bi concentration is saturated over the distance of 0.3 μm apart from the side-surface of the crack. The concentration significantly drops in the range of 0.3 μm to 0.5 μm where tiny amount of Bi was detected afterwards. This trend is opposite for the Mn concentration profile.

The MnBi layers formed at the surfaces of the cracks in the Mn powder particles were used for investigation of the diffusion coefficient (D_c) because the thickness of MnBi layers from elemental depth profiles provide an opportunity to estimate D_c. In this work, net diffusion is defined as the diffusion through a growing MnBi layer during sintering, which includes the effect of Bi flow into the Mn bulk and Mn flow towards the crack surface. The average value of D_c can be simply estimated using the diffusion relation $D_c=L^2/t$, where t and L are the diffusion duration and length, respectively (Van Nguyen and Nguyen, 2017). The diffusion length (L) is the thickness of MnBi layers measured from the cross-sectional SEM images. For each sintered MnBi powder particle shown in Figure. 4.5(b)-(d), the thickness of the MnBi layer was measured at 120 different regions over the whole area of the cross-sectional SEM images using ImageJ program (Schneider, Rasband and Eliceiri, 2012). The width of the two MnBi fringes, on opposite sides of the crack, typically differ by a factor of order ten percent (which may be a geometric factor related to the orientation of the crack relative to the cleaved surface). Accordingly, we take the average of the two fringes as a reasonable representation of the typical thickness of MnBi layers.

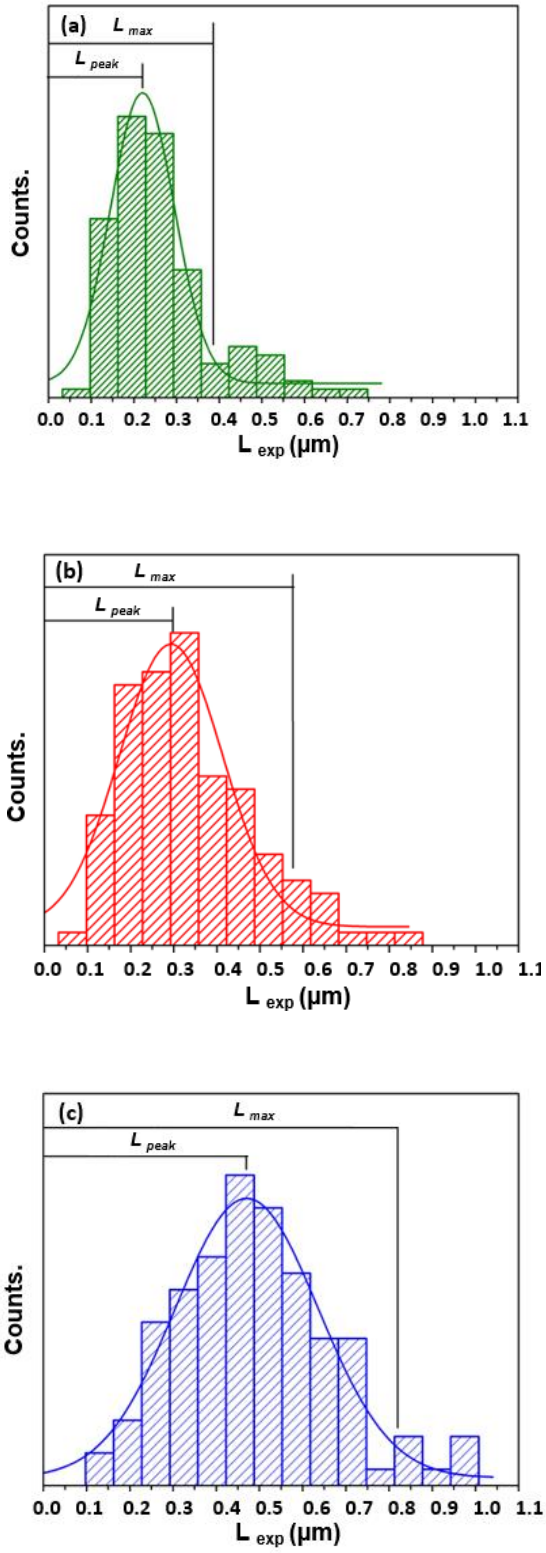

Figure 4.7 Histograms of the thickness of MnBi layers in the MnBi samples sintered at 275 °C, 325 °C and 375 °C. Each bin of the histogram is 0.05 micron.

The histograms of the measured thicknesses of the MnBi layers sintered at 275, 325 and 375 °C are shown Figure 4.7. The variation in layer thickness evident from the histograms reflects the complex nature of LPS kinetics. Indeed, the growth of layers must result from the flow of liquid Bi through irregular cracks and the resulting diffusion of Bi perpendicular to the liquid streams into the surrounding Mn landscape. It is not surprising that this process, dependent on the crack properties, on the Mn-Bi interface at the crack edges and the subsequent diffusion rate into the sample, gives rise to a range of MnBi layer growth rates. Nevertheless, the statistical properties of the distribution of layer thickness provides insight into diffusion averages in experimental conditions.

To characterize the distributions, the histograms were fitted with Gaussian distributions. The mean (L_{peak}) and standard deviation (σ) are reported in Table 4.2. The thickest MnBi layers (L_{max}) that contribute significantly to the distribution can be represented by $L_{max}=L_{peak}+2\sigma$. One might expect that such thick MnBi layers are similar to those formed on the external surface of Mn powder particles, where the growth rate is not limited by the flow of liquid Bi through the crack (i.e., when the supply of Bi is always sufficient). This suggests that L_{max} can be used as a reasonable lower-end estimate of the diffusion length D_c for the net diffusion in the sintered MnBi layer at 275, 325 and 375 °C was found to be 1.41×10^{-14}, 2.49×10^{-14} and 5.72×10^{-14} cm^2/s, respectively. The obtained D_c is of the same order of magnitude as the experimental data for other alloys reported earlier (S. Yoshida, Okumura, Kita, Takahashi and Ushioda, 2014). However, our values are up to 2 orders of magnitude smaller than that previously reported for diffusion in the arc-melted MnBi (Gupta, Anil Kumar and Khanra, 2018). This large discrepancy might be due to the difference in the material systems where large D_c in previous report was obtained by observing the change in size of Mn embedded in the arc-melted MnBi annealed at 300 °C.

One of the basic characteristics of diffusion processes is activation energy. This activation energy is generally estimated from the well-known Arrhenius equation; $D_c = D_0\exp(-E_a/K_BT)$, where D_c, D_0, E_a, K_B and T are diffusion coefficient, pre- exponential factor, activation energy of diffusion, Boltzmann constant and

temperature in Kelvin, respectively. By linear fitting of ln(D) and (1/T), the D_0 and E_a could be obtained as shown in Figure 4.8. The coefficient follows the Arrhenius equation with the pre-exponential factor of 5.33×10^{-10} cm^2/s and activation energy of 0.45 eV.

Table 4.2 The mean, standard deviation, diffusion length, and diffusion coefficient of MnBi prepared by different sintering temperatures.

Sintering Temperature (°C)	Peak position, $L_{peak} \pm \sigma/2$ (μm)	Diffusion Length, $L=L_{peak}+2\sigma$ (μm)	D_c (cm^2/s)
275	0.247 ± 0.035	0.387	3.47×10^{-14}
325	0.328 ± 0.062	0.576	7.68×10^{-14}
375	0.497 ± 0.079	0.813	15.30×10^{-14}

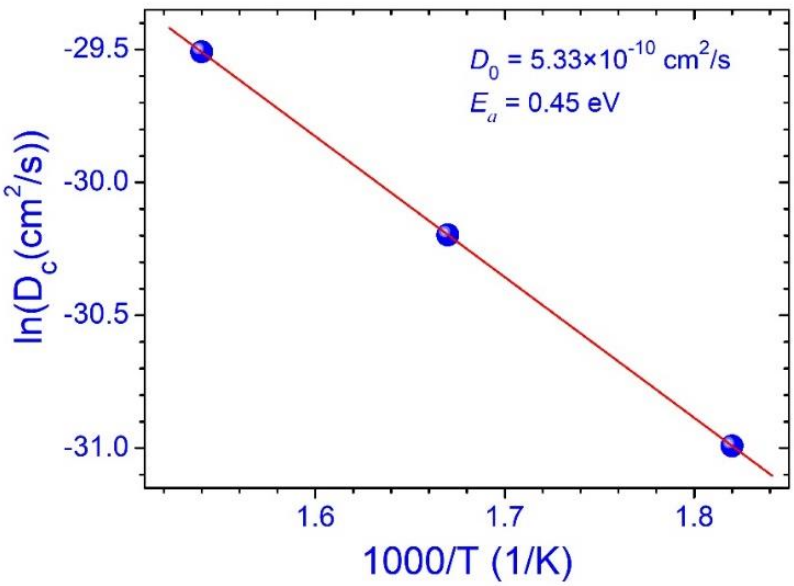

Figure 4.8 Arrhenius plot of the diffusion coefficient as a function of inverse temperature.

4.2 LTP-MnBi sintered at 325 °C for 12, 24 and 48 hours

It was shown in section 4.1 that among the three sintering temperatures, LTP-MnBi sintered at 325 °C yield the highest value of $(BH)_{max}$. In this section, the experimental results to verify that the value of $(BH)_{max}$ could still be increased when the LTP-MnBi content increases. By sintering at 325 °C with longer sintering times, the LTP-MnBi shall be produced with thicker layers and, thus, higher content of LTP-MnBi in the sintered product. In this section, the results from the investigations of the sintered MnBi products prepared at 325 °C for 12, 24 and 48 hr are reported.

4.2.1 Phase identification

Figure 4.9 shows the XRD patterns of the small MnBi powder (particle size $<$ 20 μm) and large MnBi powder (particle size of 20-53 μm) measured by using a Rigaku Smart Lab Diffractometer (Cukα, 1.54 Å) with 2θ of 20-60°. The MnBi powders were sintered at vacuum pressure below 5×10^{-7} mbar at 325 °C for 12, 24, and 48 hours, denoted as 325 °C_12hr, 325 °C_24hr, and 325 °C_48hr samples, respectively. Three main phases could be identified from the XRD patterns, which are Bi phase (card No. 96-231-0890), MnBi phases (card No. 96-900-8900), and MnO phases (card No. 96-101-0394). It is noted that MnO was also detected. This oxide was discussed in the previous section that it might be formed after the sintered product was taken out from the vacuum and exposed to air. The MnBi/Bi content ratio was estimated from the height of the MnBi and Bi intensity ratio. For the small particle size samples, the MnBi/Bi content ratio was found to be 1.68, 3.13 and 1.98 for the samples sintered for 12, 24, and 48 hrs, respectively. While the large samples, these ratios were 2.67, 4.79 and 3.40 for 12-, 24-, and 48-hr sintered samples, respectively. The two tends increase and decrease after the sintering temperatures increase. The MnBi/Bi content ratio did not increase as a linear function of sintering time as expected. This expected result is one of the issues for further study.

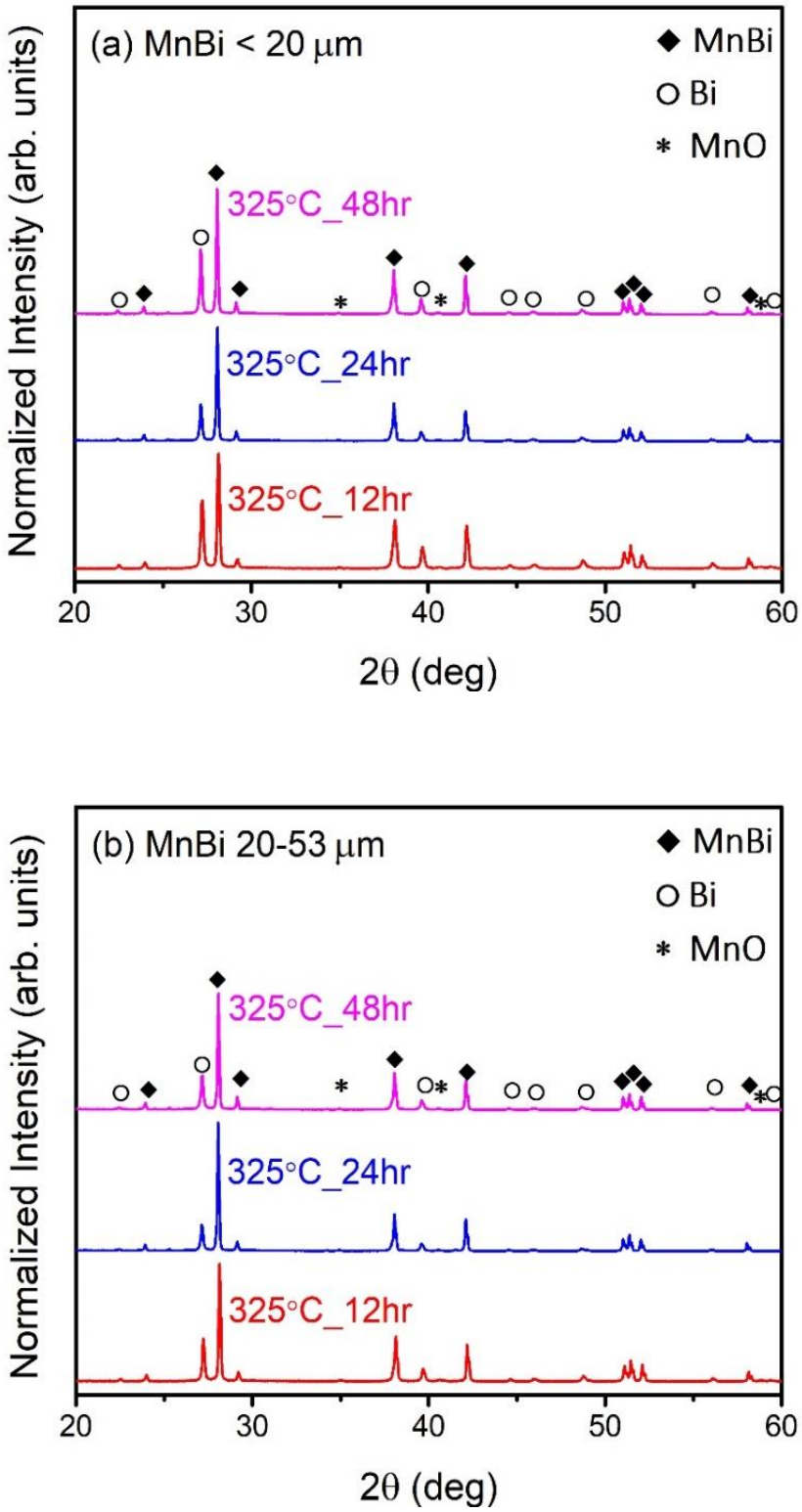

Figure 4.9 XRD patterns of the MnBi samples with (a) small particle size (< 20 μm) and (b) large MnBi particle sizes (MnBi 20-53 μm). The MnBi samples were sintered at 325 °C for 12, 24, and 48 hrs.

4.2.2 Magnetic properties

Figure 4.10 shows the room temperature M-H curves with demagnetization field correction of the MnBi powder samples sintered at 325 °C for different durations. For the sintered MnBi sample with small particle size, the H_{ci} are 4.98±0.24, 2.74±0.13 and 2.04±0.10 kOe, and M_s are 45.79±2.28, 55.07±2.75 and 55.78±2.78 emu/g for sintering times of 12, 24, and 48 hrs, respectively. For the samples with large particle size, the H_{ci} are 2.49±0.12, 1.55±0.07 and 1.71±0.08 kOe, and M_s are 54.27±2.71, 59.89±2.99 and 62.79±3.13 emu/g for sintering times of 12, 24, and 48 hrs, respectively. It is apparent that the H_{ci} decreases and M_s increases with increasing particle size. This is in an agreement with the results obtained from the MnBi samples sintered at 275, 325 and 375 °C for 12 hrs, as reported and discussed in the previous section that the lower values of H_{ci} *is* from the fact that large particles are the agglomerations of smaller particles bonded with Bi and, thus, the rotations of particles is more restricted. For the same set of sample size, the increase of M_s may be explained by the increase of LTP-MnBi content since longer sintering times result in more LTP-MnBi is formed.

It is interesting to point out the difference in shape of the M-H curves for the samples sintered for different durations. For small particle samples, the H_{ci} decreased 45% from 4.98 to 2.74 kOe when the sintering time increased from 12 to 24 hrs. However, when the sintering time increased from 24 to 48 hrs, the H_{ci} decreased only by 25% from 2.74 to 2.04 kOe. It is well understood that the value of H_{ci} increases with decreasing of MnBi particle size. For the 12-hr sintering sample, the thickness of LTP-MnBi layers formed on the exterior of the particles and interior surface on the crack surface in the particles are thinner than that for the 24- and 48-hr sintered samples. These thin layers, as compared to the magnetic domain, give rise to a higher value of H_{ci} than that for the thicker LTP-MnBi layers.

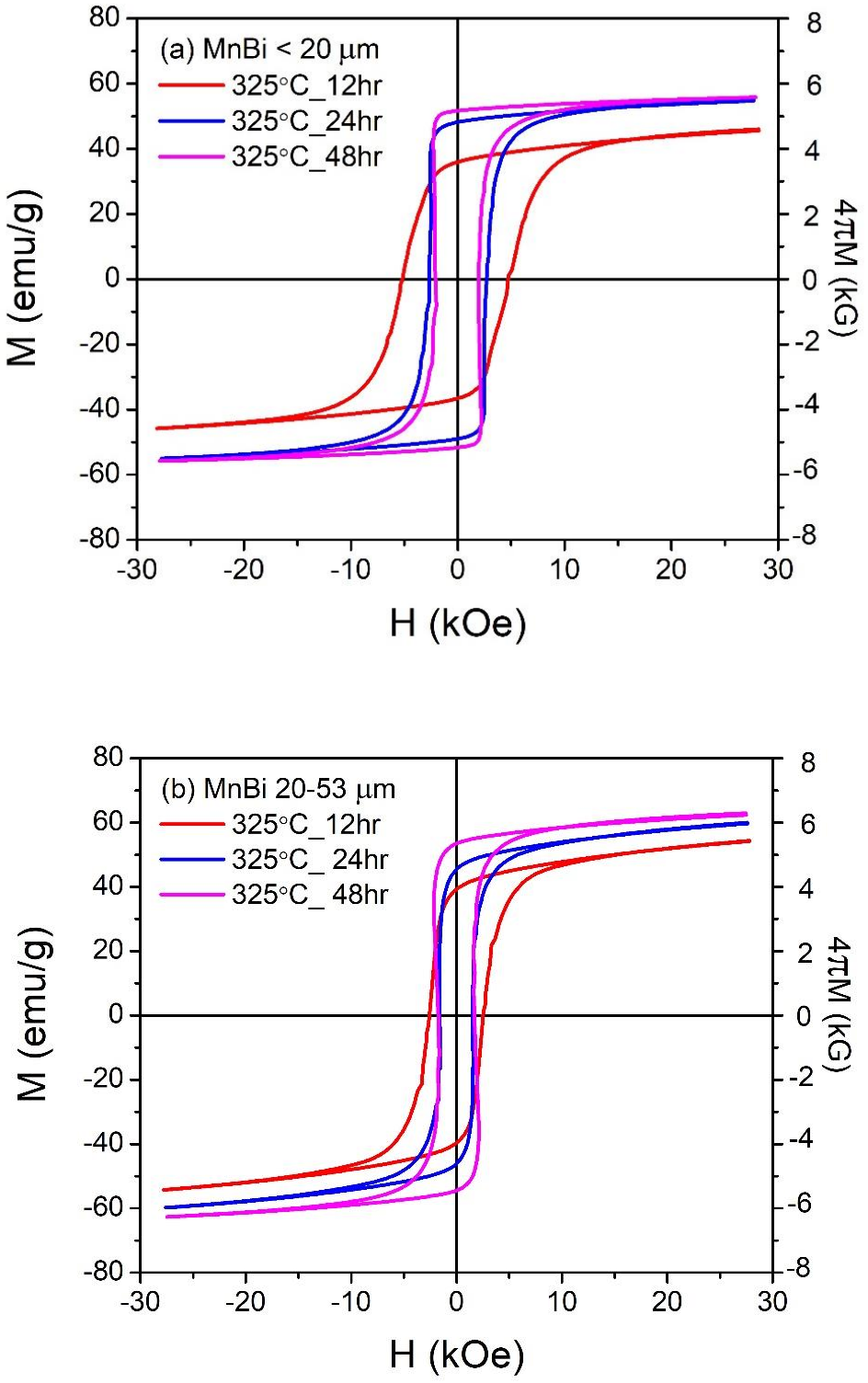

Figure 4.10 Room temperature M-H curves with demagnetization field correction of (a) the small MnBi particle size and (b) large MnBi particle size samples sintered at 325 °C for 12, 24, and 48 hrs.

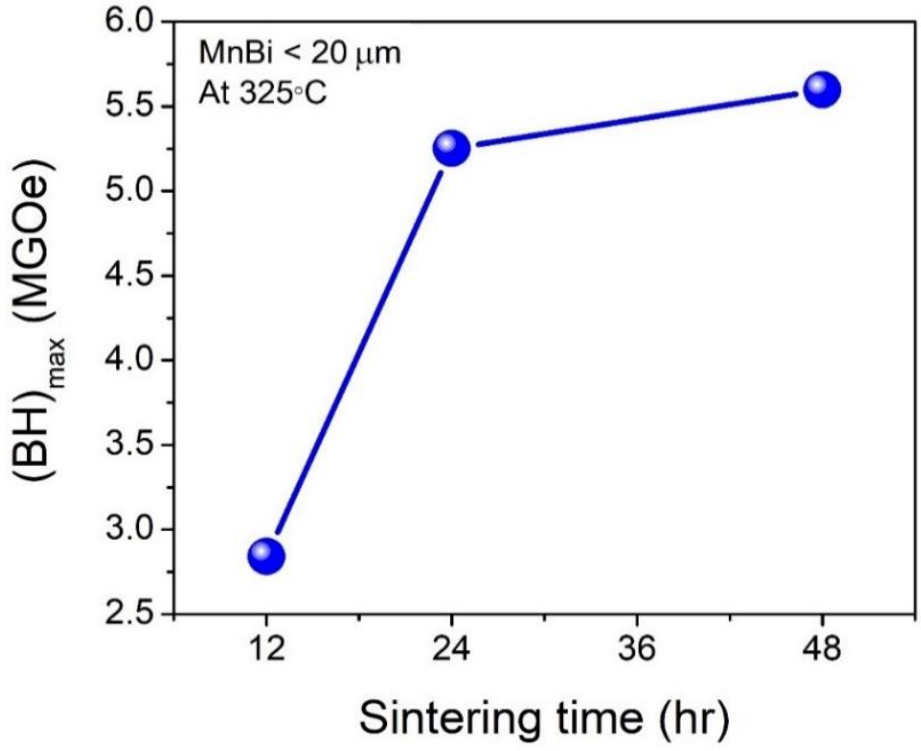

Figure 4.11 The energy product, ***(****$(BH)_{max}$*, of the MnBi samples with particle sizes less than 20 μm as a function of sintering time.

Figure 4.11 shows the value of $(BH)_{max}$ as a function of sintering time. Only the small particle size samples are of interest in order to avoid the considerations of the effects from the particle agglomerations. The energy product is in general considered as one of the performance indicators of magnetic materials and magnets. The higher energy product, the higher potential for the magnetic materials and magnets to generate energy. The values of $(BH)_{max}$ are 2.84, 5.25, and 5.59 MGOe for the samples sintered for 12, 24, and 48 hrs. This trend of $(BH)_{max}$ is similar to the trend in earlier report (Mican, Hirian, Isnard, Chicinaş and Pop, 2015). It is interesting to note that LTP-MnBi prepared in this work yields $(BH)_{max}$ for as high as those synthesized by melt-spinning process (Kim et al., 2017; Yang et al., 2012), even though the values of the melt-spinning samples were from the pre-magnetic aligned samples. This, again, confirms that the low-temperature vacuum-sintered LTP-MnBi exhibits comparable performance with other advances technique. However, the technique used in this work consumes less energy and time and can be up scale easily for mass production.

4.2.3 Diffusion in MnBi layers

A cross-sectional MnBi powder particle sintered at 325 ºC for 48 hrs, as shown in Figure 4.12(a), was prepared by an Ar ion beam slope cutting device.

The brightest areas, mostly, surrounding the MnBi powder particle are Bi. There are also the areas with brightest tone on the powder particle, which are also identified to be also Bi. This indicates that the powder particle was, in fact, partially cross-sectioned, only the central part of the particle was well cross-sectioned. More materials should have been removed to obtain good cross-sectional sample for the whole MnBi particle, however, it was not necessary for this study. The grey areas, mostly in the central part of the particle, are the un-interacted Mn. MnBi observed on the sample were from the MnBi formed at the exterior surface of the Mn particle, seen as the bright continuous area on the outer part, and the MnBi formed at the side-surfaces of the crack in the Mn powder particle, seen as a spider-web feature extending from the outer to inner parts. The formation of the MnBi layers on the crack surfaces were observed as two bright stripes sandwiching the crack, as shown in the higher resolution SEM images in Figure 4.12(b), (c), and (d) for the particle samples sintered at 325 ºC for 12, 24 and 48 hrs, respectively. The processes involving this formation of MnBi were discussed in the previous section. The main mechanism for controlling the thickness of these MnBi is diffusion Mn and Bi through the forming MnBi layer. As expected, a longer sintering time, the thicker MnBi layer was formed. This is of course the result from the diffusion limited mechanism. The symmetry of the MnBi layers observed was the resulted from the fact that the crack surface was not perpendicular to the surface of the cross-sectional sample (Borsup et al., 2022).

The same method, as employed in the previous section, for estimating the thickness of the MnBi layers form on the inside surface of the crack was carried out. Figure 4.13(a), (b), and (c) show the histogram of the thickness of the MnBi layers formed on the crack surfaces for the particles sintered at 325 ºC for 12, 24, and 48 hrs, respectively. Each histogram was obtained from measuring the zoom-in SEM image as shown in Figure 4.12 for a total of 120 data points using the program Image J (Schneider et al., 2012).

Then, the histograms were fitted with a Gaussian function. The average diffusion length was estimated to be $L_{peak} + 2\sigma$, where L_{peak}, σ are the peak position and the standard deviation of the Gaussian function, respectively. The results were used to calculate the mean, standard deviation, and a maximum MnBi layer thickness as shown in Table 4.3.

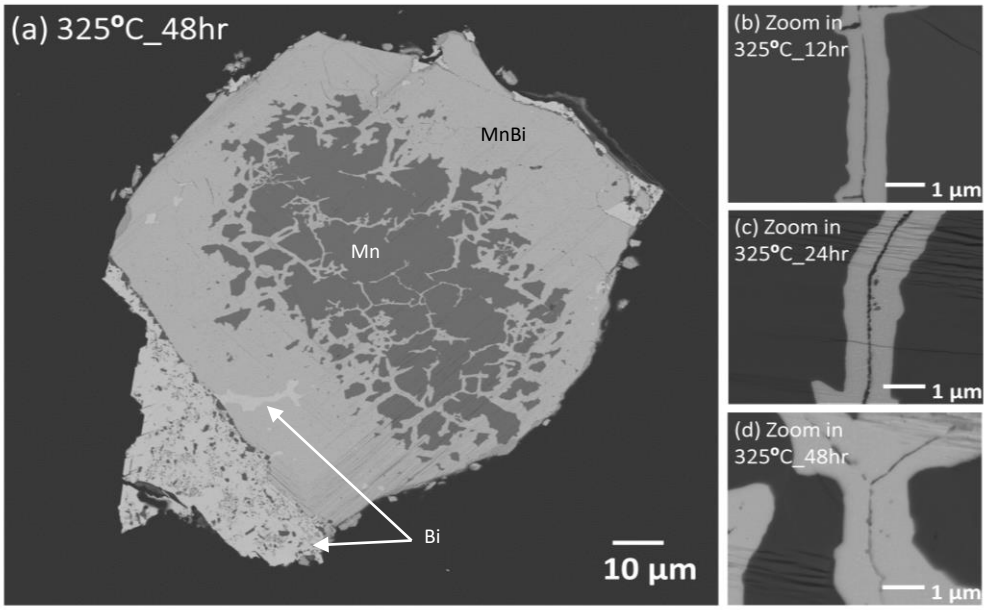

Figure 4.12 (a) A cross-sectional MnBi powder at 325 °C for 48 hr was prepared by ion beam slope cutting device and the zoom-in SEM images of a cross-sectional MnBi powder in the (b) 325 °C_12hr, (c) 325 °C_24hr, and (d) 325 °C _48hr at nearly the crack, respectively.

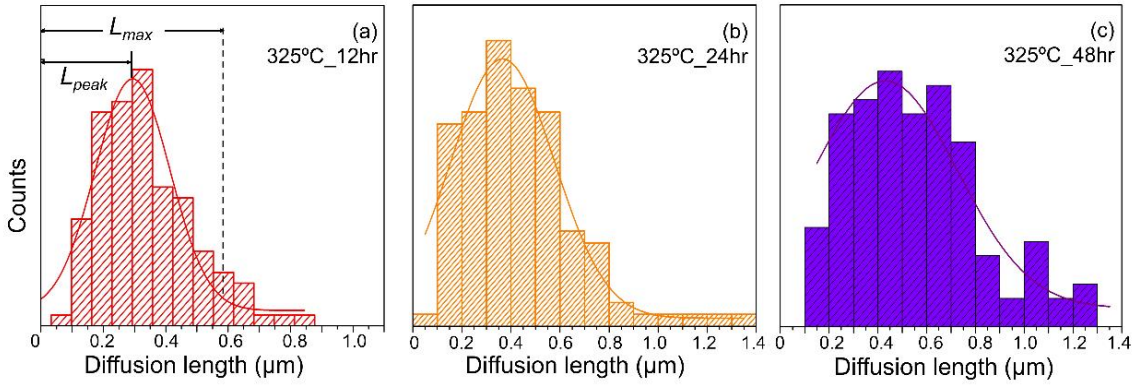

Figure 4.13. Histogram of the thickness of MnBi layers in the (a) 325 °C_12hr, (b) 325 °C_24hr, and (c) 325 °C _48hr. Each bin of the histogram is 0.05 µm.

Table 4.3 The mean, standard deviation, and the maximum MnBi layer thickness prepared at different sintering time.

ID Sample	Peak position, $L_{peak} \pm \sigma/2$ *(μm)*	Diffusion length, $L_{max} = L_{peak} + 2\sigma$ *(μm)*
325 °C_12hr	0.328±0.062	0.576
325 °C_24hr	0.366±0.105	0.786
325 °C_48hr	0.431±0.148	1.023

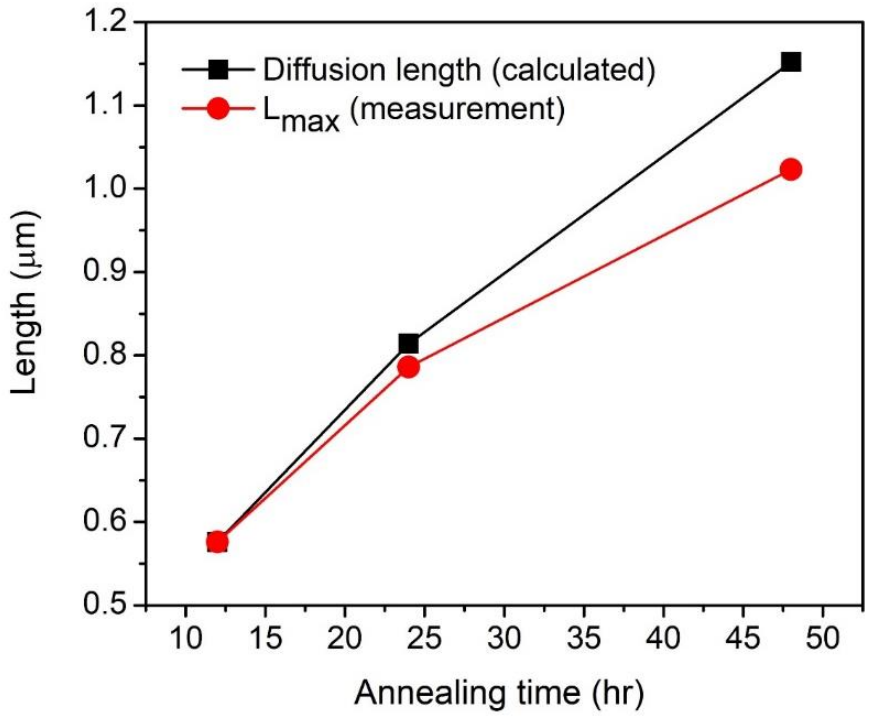

Figure 4.14 Comparison of calculating MnBi layer thickness in the 1st order diffusion equation and experimental MnBi layer thickness prepared at 325 °C for 12hr, 24hr, and 48hr, respectively.

Figure 4.14 presents the comparison of the MnBi layer thickness calculated from the first order diffusion equation and the experimentally measured MnBi layer thickness formed by sintering at 325 °C for 12, 24, and 48 hrs. In previous section, the diffusion coefficient of the MnBi powder (D_c) were deduced from the samples sintered at 275, 325 and 375 °C for 12 hrs. $D_c = L^2/t$ where t is a duration time and L is the diffusion length or the MnBi layer thickness. The D_c values were 3.47 x 10^{-14} cm^2/s, 7.68 x 10^{-14} cm^2/s, and 15.30×10^{-14} cm^2/s for sintering temperatures of 275 °C, 325 °C, and 375 °C, respectively. With the known diffusion coefficient, the diffusion length or the thickness of the MnBi layers could be calculated from the relation $L = \sqrt{(D_c\, t)}$. The calculated MnBi layer thickness values were 0.576 μm, 0.814 μm, and 1.152 μm for the samples with sintering time 12, 24, and 48 hrs, respectively. The calculated values were close to the experimentally measured MnBi layer thicknesses which were 0.576 μm, 0.786 μm, and 1.023 μm. There is the difference in the calculate and measured values, and the difference increases with sintering time. This might be that the 1st order diffusion equation may not be adequate for prolonged sintering. The 1st order diffusion equation is generally accurate for diffusion in a short distance or short diffusion time. That is the case shown in the figure.

4.3 Long-term stability of LTP-MnBi

The product from liquid-phase sintering a mixture of Mn and Bi powders at low-temperature in vacuum composed LTP-MnBi, Bi and Mn. Thermal stability of this sintered product is of great important for future utilizations. This section reports the changes in magnetic property, structures and chemical of the sintered product over an extended period. Mn and Bi powder with atomic ratio of 1:1 was mixed and sintered at 275 °C for 3 hrs in vacuum. The particle size of Mn powder was below 20 μm. After sintering, the sample was ground and sieved to select powder particles with size of less than 20 μm. The fresh and 18-month-old MnBi samples were investigated by different characterization techniques i.e., VSM, XRD, SEM/EDS, and XAS. The 18-month-old MnBi sample was the sintered MnBi powder packed in a sealed tube, which is in fact a sample container of the VSM system.

4.3.1 Magnetic properties

The room temperature M-H curves with demagnetization field corrector of the MnBi powder stored in a sealed tube as a function of storing time are shown in Figure 4.15. The important parameters of the magnetic property are given in Table 4.4. It is noted that sealing of the VSM container is not vacuum sealing, it is just an ordinary lid of a plastic container. For over the 18 months, the sample was always kept in the tube. It is obvious that there were almost no changes in the M-H curve after the sample was stored for 2 months. The dramatic changes were observed when the sample was 7 months old. Both coercivity and remanent magnetization increased by approximately 30%. After storing for another 7 months, the coercivity and remanent magnetization kept increasing but with lower increasing rates. For the 18 months old sample, the coercivity increased but the remanent magnetization decreased slightly as compared to the 14 months old sample. It is interesting to note that, for the whole storing period of 18 months, the energy product increase with storing time while the saturated magnetization remained almost unchanged, very slight reduction though. The change pattern of the M-H curve for MnBi have not been reported before. Thus, it was worthwhile for in-depth investigations to understand physics behind the change.

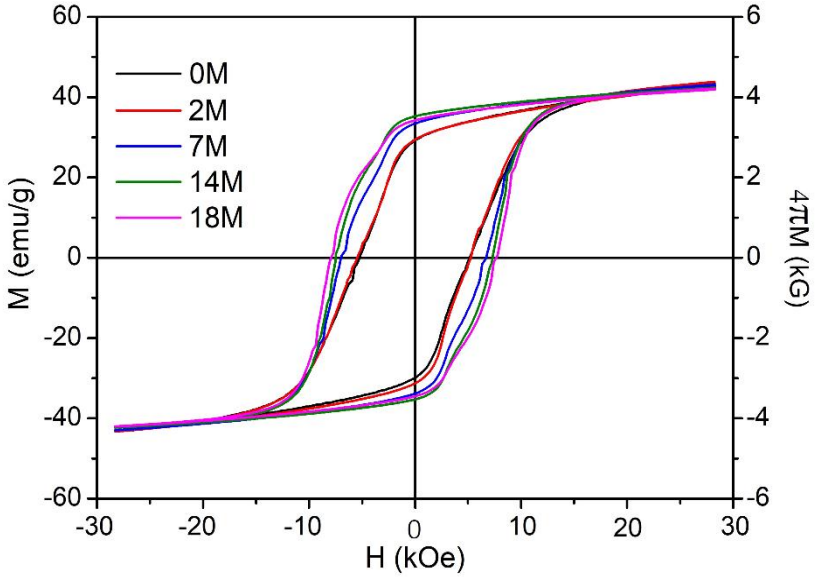

Figure 4.15 Room temperature M-H curves with demagnetization field correction of the samples stored in a sealed tube up to 18 months.

Table 4.4 Magnetic properties (H_c, M_s, $(BH)_{max}$) of MnBi sample at different ages or storing periods.

Sample or ID/Storing time	H_{ci} (kOe)	M_s (emu/g)	$(BH)_{max}$ (MGOe)
0M	5.15±0.26	43.23±2.16	1.77
2M	5.34±0.27	43.21±2.16	1.92
7M	6.87±0.34	43.05±2.15	2.50
14M	7.43±0.37	42.34±2.11	2.84
18M	7.81±0.39	41.98±2.15	2.70

4.3.2 Surface morphology of LTP-MnBi powder

Figure 4.16(a) and (b) are SEM micrographs showing the morphology of the fresh and 18-month-old MnBi powder samples. The analysis of particle size was carried out by using the ImageJ software. It was found that the average particle size of the MnBi powder increased from 9.7 μm for the fresh sample to 33.9 μm for the 18-month-old sample, as seen in Figure 4.16(c) and (d). This scenario could be expected by the nature of small and light particles with high magnetic strength. The substantial of large particle size may occur by self-magnetic attraction assisted by environmental humidity and sample storage. There are additional factors playing an important role in the 18-month-old sample. Figure 4.16(a1) and (a2) show the zoom-in SEM image of the individual MnBi particle, respectively. The selected two areas of EDS square scan were presented in Figure 4.16(e). The quantities results of EDS square analysis for the fresh sample and 18-month-old are composed of Mn, Bi, and O elements. The atomic percentage of O increased from 12.73% for the fresh sample to 35.30% for the 18-month-old sample. The atomic percentage trend of O increases while Mn decreases, and Bi remains almost unchanged. The Mn fluctuates with O more than Bi, indicating that Mn is highly sensitive to oxygen.

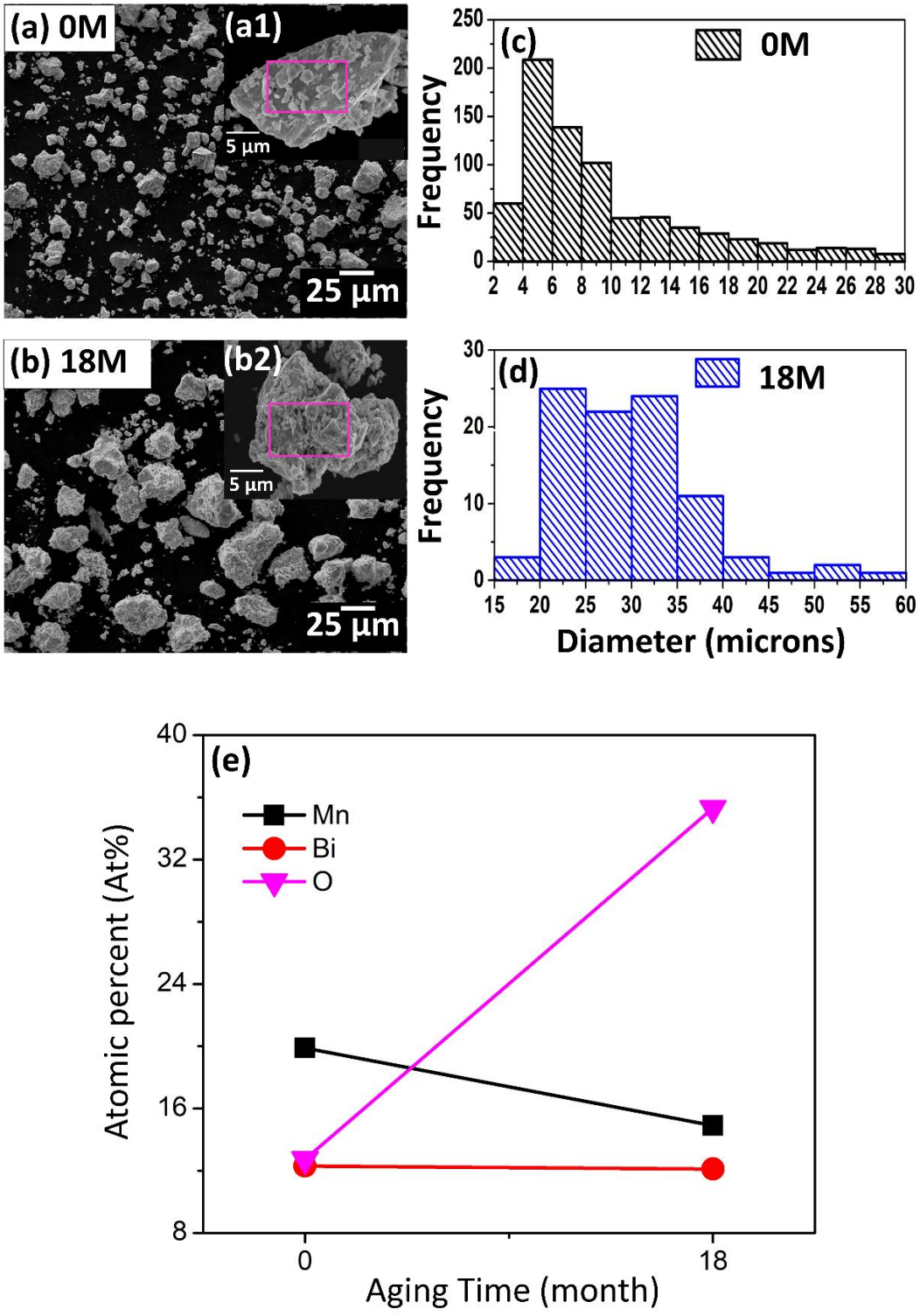

Figure 4.16 SEM images of (a) fresh and (b) 18-month-old MnBi powders. The particle size distribution of MnBi powders shown in (c) and (d). The red squares in (a) and (b) are the areas for EDS measurements to determine the elemental composition, as shown in (e).

4.3.3 Phase identification

XRD measurements and analysis were performed to identify not only the phase structure but also the degree of randomly phase distribution. As seen in Figure 4.17(a), the wide scan XRD patterns of all samples present the dominant peaks of MnBi phase (card No. 96-900-8900) and Bi phase (card No. 96-231-0890) as well as tiny peaks of Mn phase (card No. 96-901-1109) and MnO phase (card No. 96-101-0394). The crystallite size (*D*) can be calculated by full width with half maximum (FWHM; *B*) with formula is ($D = \frac{K\lambda}{BCOS\theta}$), where is *K* = 0.9 is shape factor constant. The crystallite size and FWHM are 51.75 nm, 35.53 nm, and 0.17 deg., 0.26 deg. for the fresh and old samples, respectively. The old sample had a smaller crystallite size than the fresh sample. The percentage of crystallinity of two samples are 93.64% and 85.86%, respectively. They can be estimated by Integral Gaussian fitting of peak (sum area/area all of peak*100). This is a very clear evidence result that sample exposure to air can be found slightly low crystallinity.

After exposing to the air of up to 18 months, the XRD patterns are rather similar to the fresh sample indicating the robustness of our LTP-MnBi prepared by vacuum sintering which is in contrast to other reports (Janotová et al., 2018; M. Y. Sun et al., 2016; Villanueva et al., 2019). It is noticeable that the ratio of the main Bi (θ~27°) and MnBi (θ~28°) peaks of the old sample is distinct from the fresh sample. This result has been described elsewhere by the role of randomly magnetic distribution (RMD) (V. Nguyen et al., 2014).

The degree of RMD can be determined by the relative intensity ratio (γ) between the out-of plane and in-plane XRD peaks commonly be referred to the MnBi (002) and MnBi (101) with angle of 28.2 and 29.2 degrees, respectively. A formula is $\gamma = (\frac{I(MnBi(002)}{I(MnBi(101))[0.102]})$, where a fully isotopic MnBi powder of theoretical value is 0.102 (Poudyal et al., 2016; Truong and Vuong, 2015).

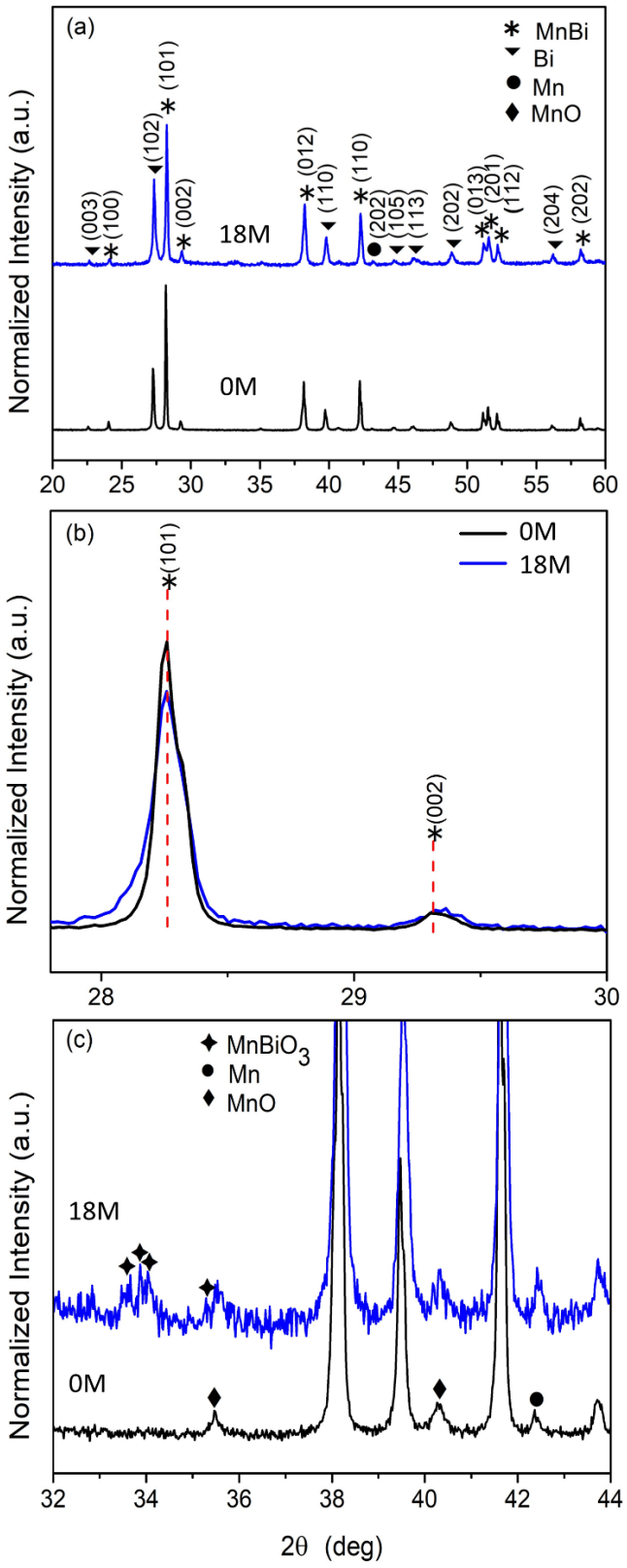

Figure 4.17 XRD patterns of the fresh and 18-month-old LTP-MnBi showing at different 2θ ranges (a) 20-60 deg. (b) 27.79 – 30 deg. And (c) 32 – 44 deg.

The zoom-in XRD patterns between 2θ = 25 °- 30° are shown in Figure 4.17 (b), where γ can be calculated to be 0.71 and 0.84 for the fresh and 18-month-old samples, respectively. The 18-month-old sample possesses the higher γ indicating better magnetic self-alignment as compared to the fresh sample. This result may be caused by the storage environment of the 18-month-old sample which was squeezed in the limited space and aligned multiple times during VSM measurements. The degree of magnetic self-alignment is strongly related to H_{ci} (Poudyal et al., 2016). In principle, if the sample is better aligned, higher force is required to flip the magnetic domain than the randomly aligned sample resulting in higher H_{ci} (Jain, 2010). This would describe the enlargement of H_{ci} in the 18-month-old sample (Figure 4.15). In view of oxidation, the zoom-in XRD patterns near the baseline are presented in Figure 4.17 (c). Some additional tiny peaks (assigned to $MnBiO_3$ (card No. 96-434-0613) and MnO phases) were revealed in 18-month-old samples. The low oxides contents could be described by the low free-Mn content on the surfaces which is the advantage of the LTP-MnBi prepared by vacuum sintering. A similar result with Yoshida et.al were observed, they found a low free-Mn content in MnBi ingot at zone-melting, the selecting temperature prepared during phase transformation of HTP to LTP (H. Yoshida, Shima, Takahashi and Fujimori, 1999).

4.3.4 Local structure of Mn atoms

The X-ray absorption (XAS) technique was used to determine the changes of local structure and the oxidation around Mn atoms of the MnBi samples. The experimental and theoretical results of XAS measurement were analyzed by ATHENA software (Ravel and Newville, 2005) and the Feff code version 9 (Rehr, Kas, Vila, Prange and Jorissen, 2010).

Figure 4.18(a) shows the simulated MnO and MnBi XANES spectra. It was found that MnBi possesses broader spectrum with higher positions of the edge-shift and the highest peak energies than MnO. Figure 4.18(b) represents a consistency between our measured Mn K-edge XANES spectrum of the 0M sample and the MnBi:MnO (1:1) linearly combined spectrum. This feature refers to the initial composition of MnO which may cause to the low magnetic performance of our as-prepared sample.

Figure 4.18(c) shows the Mn K-edge spectra of the fresh and 18-month-old samples as well as the standard Mn-foil (Mn^0) and MnO (Mn^{2+}) spectra. It was found that XANES spectra of all samples are similar to the MnO confirming oxides were initially formed on the fresh MnBi samples. The absorption edge of 18-month-old sample seems to be unchanged. The white-line intensity of 18-month-old sample was lower compared to the fresh one indicating more oxidation upon aging.

To better understand such behavior, the Fourier transform magnitude in r-pace of experimental and standard samples were computed from EXAFS spectra and represented in Figure 4.18(d). The curves of all samples were closed to the MnO than Mn spectra. We focus on the first Mn-O and Mn-Mn shells which were assigned peak position at R = 1.6 and 2.6 Å, respectively (Nieminen et al., 2019). Interestingly, The Mn-Mn bond of the 18-month-old sample is located at the same position but its Mn-O bond is shifted outward from the reference. This may be implied that the 18-month-old was a small amount of oxidation. We have not an experimental fingerprint of LTP-MnBi to reference the 18-month-old sample. LTP-MnBi is the hexagonal NiAs ($P6_3/mmc$) structure (Bandaru, Sands, Weller and Marinero, 1999). The calculated Mn-Bi bonded lengths are 2.88 Å (Persson, 2016), which is close to Mn-Mn peak as seen in Figure 4.18(d). Hence, the MnBi powder stored in the 18-month-old sample has virtually no degradation. The oxide layer only occurs on the surface (Mn-O bonding) while the Mn core is unchanged (Mn-Mn bonding) upon aging.

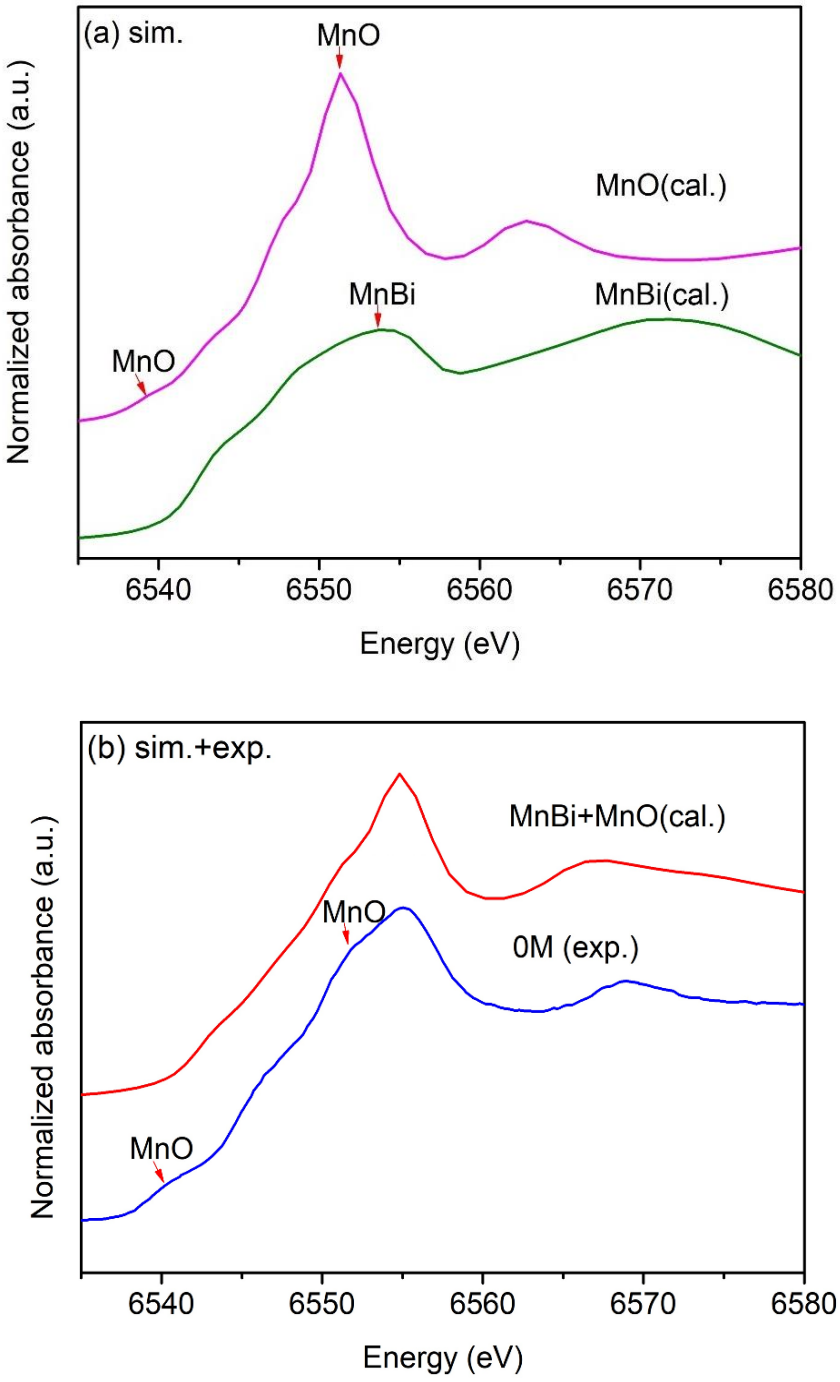

Figure 4.18 (a) Theoretical K-edge XANES spectra of MnO (cal.) and MnBi (cal.), (b) the comparison of theoretical XANES spectrum for MnBi+MnO and experimental XANES spectrum of fresh MnBi, respectively, (c) Mn K-edge XANES spectra of LTP-MnBi and standard samples, (d) Fourier transform of EXAFS spectra of previous samples (fresh MnBi, old MnBi, and standard samples).

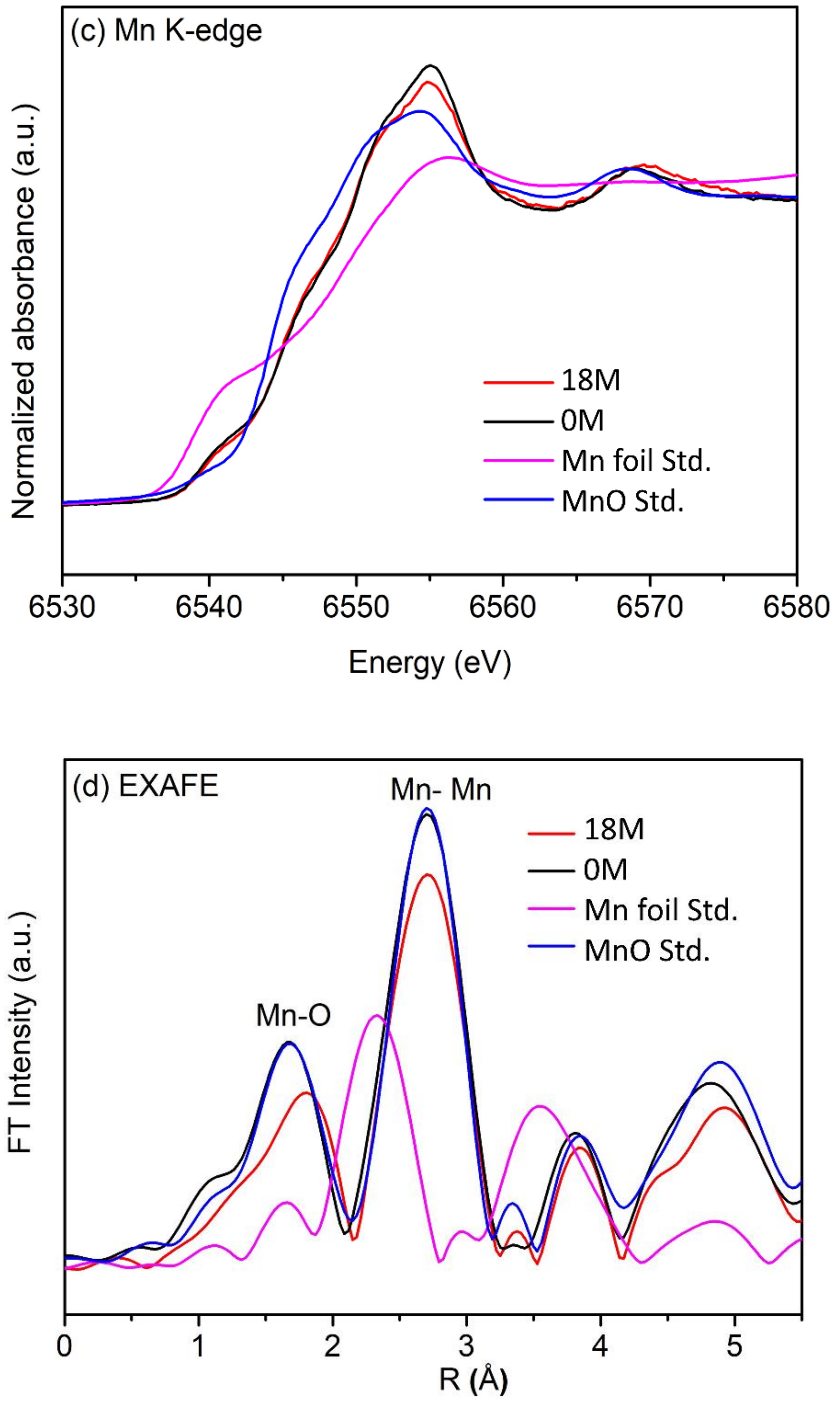

Figure 4.18 (Continue) (a) Theoretical K-edge XANES spectra of MnO (cal.) and MnBi (cal.), (b) the comparison of theoretical XANES spectrum for MnBi+MnO and experimental XANES spectrum of fresh MnBi, respectively, (c) Mn K-edge XANES spectra of LTP-MnBi and standard samples, (d) Fourier transform of EXAFS spectra of previous samples (fresh MnBi, old MnBi, and standard samples).

In this part, the diffusion mechanism is introduced as a key role to explain overall experimental results analytically and logically. Since an increase of $(BH)_{max}$ and the opposite tendency of Fourier transform magnitude in r-pace could not be interpreted without adding this term. As mentioned in our previous work (Borsup et al., 2022), the formation of LTP-MnBi during vacuum sintering were described by the diffusion mechanism. The MnBi concentration is directly related to the diffusion length which can be calculated using the diffusion relation $D_c = L^2/t$, where t and L are the diffusion duration and length, respectively (Van Nguyen and Nguyen, 2017). Because the sample reported in this work were sintered at 275 °C for only 3 hr, the $(BH)_{max}$ of 68.50 % compared to our previous work (sintered at 275 °C for 12 hr) is reasonable. Applying the diffusion coefficient of 3.47×10^{-14} cm^2/s (at 275 °C), the calculated diffusion length of 204 nm has been obtained for the fresh sample. This is about 53% of the diffusion length reported earlier (L_{max} = 387 nm) which is quite consistent with its $(BH)_{max}$.

From the fact that the diffusion process can be continued in much lower rate even at room temperature. By applying Arrhenius plot of activation energy, the diffusion coefficient can be calculated to be 1.45995E-17 cm^2/s at room temperature. An additional diffusion length of 260 nm can then be obtained after storing in the VSM sample container for 18 months. Hence, overall diffusion length could be estimated, by the summation between initial and additional lengths, to be 464 nm. This value is closed to those obtained in previous work with comparable $(BH)_{max}$, as depicted in Figure 4.19. The $(BH)_{max}$ of the 18-month-old sample increases from fresh to 14-month-old samples. The highest $(BH)_{max}$ was observed in the 14-month-old sample whose is then slightly dropped after 18 months. This is due to the large number of magnetic domains in the MnBi layer, as the thickness of MnBi layer increases with increasing aging time, increasing H_{ci} and in part due to the oxide formation affects to the degradation of MnBi magnet exposed to air.

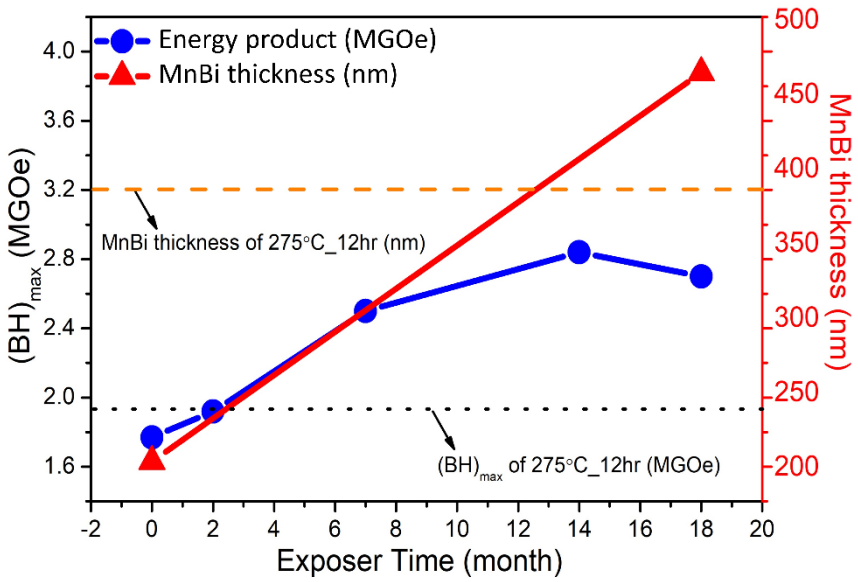

Figure 4.19 Discussion: a relationship of the maximum energy product and diffusion length with a difference period.

4.4 Decomposition of MnBi at 150 °C

This section reports the study of decomposition of LTP-MnBi at elevated temperature. LTP-MnBi powder was prepared at 275 °C for 12hr. After sintering, the samples were heated at 150 °C for different duration in an oven atmosphere (0, 0.5, 3, 6, 12, 24, and 48hr). Annealing time was used as an aging accelerator to monitor the degradation. The ID samples were formatted as MnBi_time. For example, MnBi_48 is the sintered MnBi sample that was heated at 150 °C for 48 hr. Then, the properties of their samples heated at various duration were characterized by several techniques; SEM/EDS, XRD, VSM, and XANES have presented in the details below.

4.4.1 Surface morphology and chemical composition

Figure 4.20 shows the SEM images and their corresponding colors (inset) of the LTP-MnBi powder heated at 150 °C for different periods of time. The surfaces of MnBi_0 was contributed with the white and grey areas, corresponding to the Bi and MnBi phases which are detected by EDS analysis, as seen in Figure 4.20(a). The excess of liquid Bi on the surfaces can be understood as the residue of incomplete diffusion

process during liquid-phase sintering (LPS) (Van Nguyen and Nguyen, 2017). The average particle size of the sintered sample is 20 um which is approximately three times larger than the milled-Mn particles (~9 μm) resulting from the Mn-Bi densification during LPS. It is seen that the proportion of Bi phase decreases as a function of heating time (reduction of white area ratio) where most of the Bi areas are obviously appeared as white circular particles labelled by green narrow. As a function of heating time, the oxygen content increases as seen in points A and D of Figure 4.20(h). In addition, point C has more Mn than point B, resulting in a higher oxygen content. This could be described by the reactive nature of Mn which is oxidized much easier than Bi.

By considering the colors at each condition, the MnBi_0 possesses the light brown color which is rather similar to the starting Bi powder. This is possibly related to the numerous coverages of Bi on the surfaces as seen in the SEM image (Figure 1(a)). Its color turns to darker brown and then navy blue after 0.5 and 3 hr heating time, respectively. The color slightly changes to dark green afterwards, however, not obvious. The changes in sample's color might be described by the formation of manganese oxide in different oxidation states. For example, the Mn^{2+} is pale pink, Mn^{4+} is brown/black and Mn^{6+} is green. 3+, or any incorrect color. (Received from https://www.chemicool.com/elements/manganese.html). The striking color changes are consistent with the domination of oxide areas as seen in the SEM image.

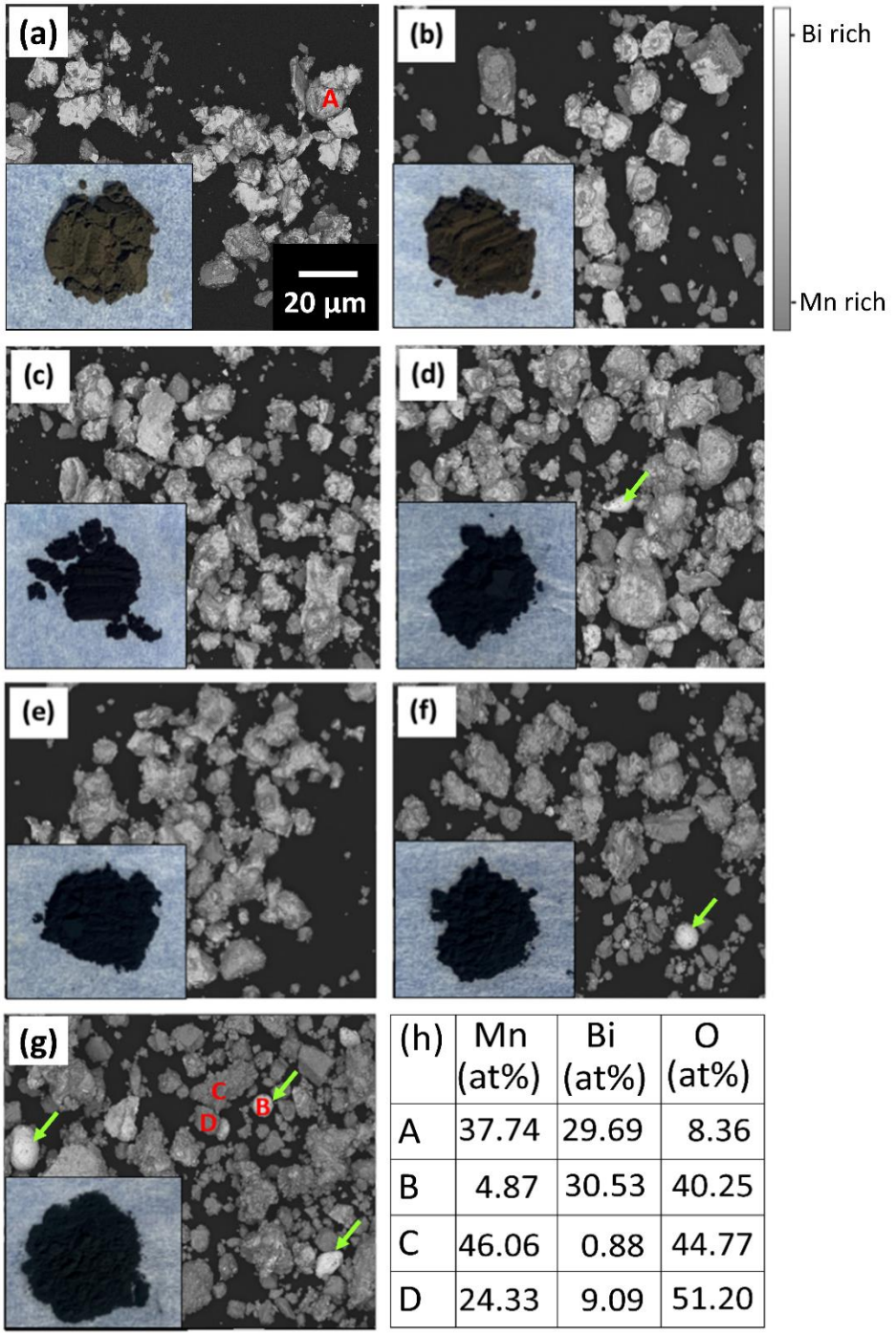

(h)	Mn (at%)	Bi (at%)	O (at%)
A	37.74	29.69	8.36
B	4.87	30.53	40.25
C	46.06	0.88	44.77
D	24.33	9.09	51.20

Figure 4.20 SEM images of LTP-MnBi powder heated at 150 °C at different duration; (a) 0, (b) 0.5, (c) 3, (d) 6, (e) 12, (f) 24, and (g) 48hr. Inset shows their corresponding colors of all samples, and the specific points of EDS analysis (A, B, C, and D) in (h).

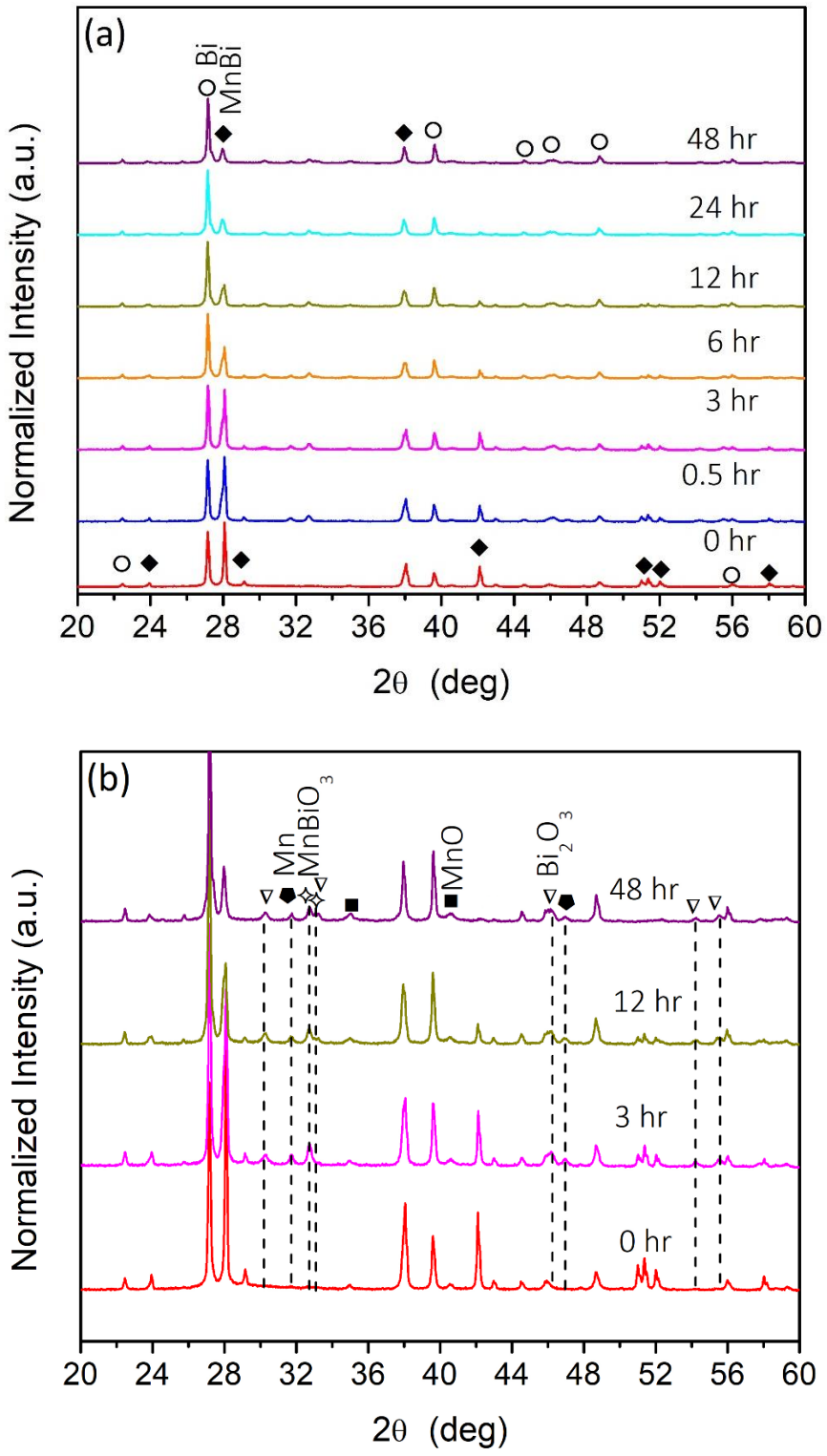

Figure 4.21 (a) X-ray diffraction patterns of LTP-MnBi powder heated at 150 °C for different duration. (b) The zoom-in patterns of selected conditions revealing several forms of impurities.

4.4.2 Phase identification

The XRD patterns of MnBi samples after thermal annealing as a function of heating duration and the zoom-in XRD patterns of selected conditions revealing several forms of impurities are shown in Figure 4.21(a) and Figure 4.21(b), respectively. The as-sintered sample (red spectrum) has mainly contained MnBi (card No. 96-900-8900) and Bi phases (card No. 96-231-0890), also including to the tiny peaks of MnO phase (card No. 96-101-0394). After heating duration, the intensity of MnBi main peaks decreased whereas the Bi and Mn peaks experienced an increase as a function of heating time. The oxide peaks were 2θ = 30.27, 31.75 32.76, 33.18, 46.17, 46.96, 54.23 and 55.5 deg, which indicated by the vertical black dot. The tendency of those peaks increased with increasing heating time. Those peaks corresponded to MnO (card No. 96-101-0394), $MnBiO_3$ (card No. 96-434-0613) and Bi_2O_3 (card No. 01-074-1375) phases, respectively. The percentage of MnBi concentration were calculated approximately using the relative area ratio between the intensity of main MnBi and Bi peaks (2θ = 27.27 and 28.07 deg, respectively) to be 51.9, 48.8, 40.8, 31.7, 23.6, 15.8 and 12.4 wt% for MnBi_0, MnBi_0.5, MnBi_3, MnBi_6, MnBi_12, MnBi_24 and MnBi_48, respectively. However, the oxide content is relatively low, not more than 5% of MnBi_48. The oxide formation was likely formed at the surface. The high residual Bi content is due to the fact that Bi is more difficult to oxidized than Mn (Villanueva et al., 2019). The XRD results support the MnBi decomposition, Mn and Bi segregated from MnBi during heating, leading to MnBi phases decreased (J. Cui et al., 2014).

4.4.3 Chemical composition

Figure 4.22 shows the Mn-K edge XANES spectra of the selected conditions (MnBi_0, MnBi_12 and MnBi_48), references spectra (MnO and Mn_2O_3), and the old theoretical results of calculated MnBi in Feff code version 9 (Rehr et al., 2010). It can be seen that the edge energy and lineshape of the as-prepared sample is similar to the reference for both MnO and MnBi (cal.), indicating that the MnBi oxidation state is close to Mn^{2+}. The edge energy of all experimental spectra was slightly shifted to Mn_2O_3 reference (Mn^{3+}) and the whiteline increased as elevated heating duration implying an increase of oxides.

The changes in oxidation states of the aged samples were determined by using the linear interpolation between edge energy of MnO (Mn^{2+}, edge energy = 6544 eV) and Mn_2O_3 (Mn^{3+}, edge energy = 6548 eV). The oxidation states were calculated by the form: $x = 3 - z$, where x is oxidation state, and z is a MnO fraction (the 100% of MnO faction = 1 at edge energy of 6544 eV.) Note that, only the MnO fraction were used as qualitative oxidation state determination and we admitted that other forms of manganese oxides are also expected in the heated sample. The calculated oxidation states are 2, 2.75 and 3 for MnBi_0, MnBi_12 and MnBi_48, respectively.

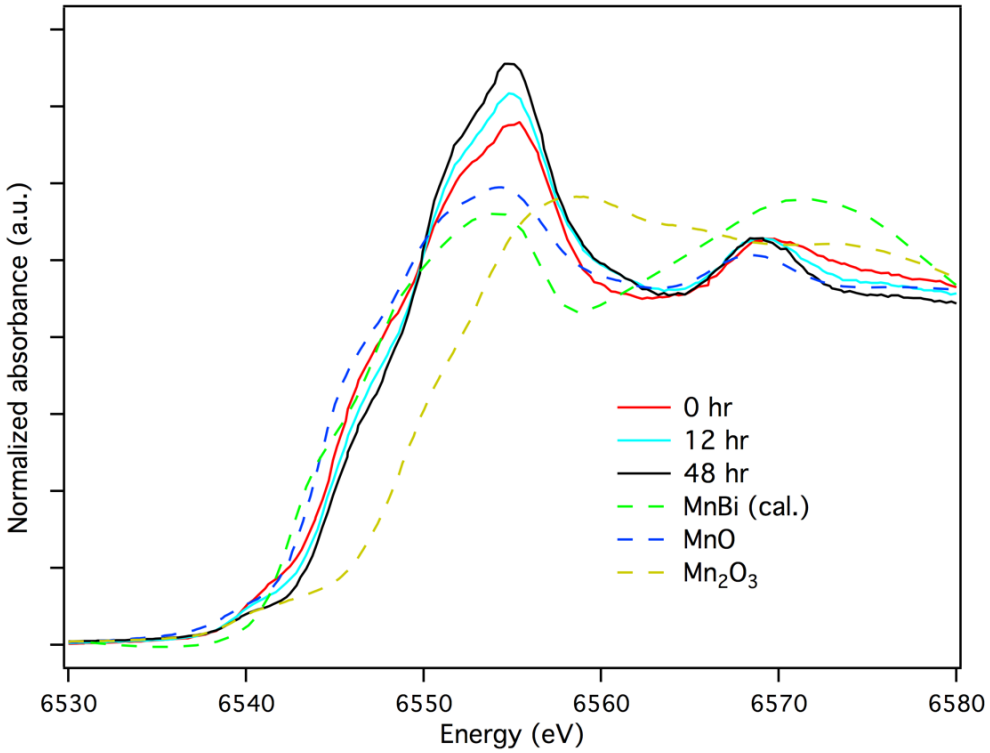

Figure 4.22 The Mn K-edge XANES spectra of MnBi powder heated at 150 °C for different duration. Dashed lines represent MnO, Mn_2O_3 and calculated MnBi spectra.

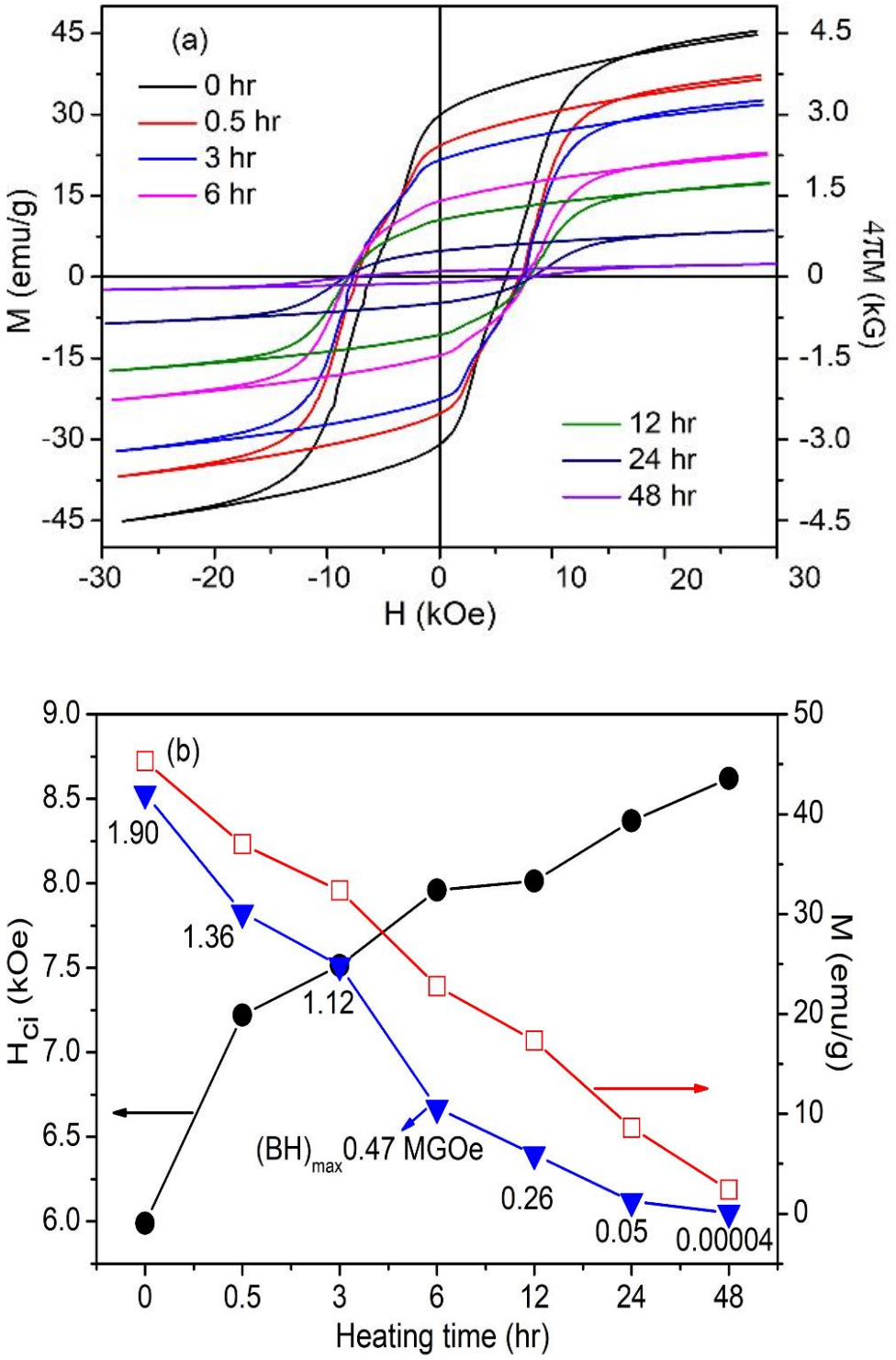

Figure 4.23 (a) Room temperature M-H curves with demagnetization field corrector of MnBi powder heated at 150 °C for different duration. (b) Extracted saturation magnetization (M_s), coercivity (H_{ci}) and the calculated energy products ($(BH)_{max}$).

4.4.3 Magnetic properties

The magnetic properties of MnBi powder heated at different duration were studied by VSM. The room temperature M-H curves with demagnetization field of MnBi powder at different conditions were plotted in Figure 4.23(a).

Their corresponding magnetic values including saturation magnetization (M_s), coercivity (H_{ci}) and energy products ($(BH)_{max}$) were presented in Figure 4.23(b). The magnetic properties of the as-fabricated sample are M_s = 45.31 emu/g, H_{ci} = 5.98 kOe and $(BH)_{max}$ = 1.90 MGOe. A comparison of $(BH)_{max}$ between MnBi_0 and the small MnBi-275 °C for 12 hr (Table 4.1) is 12.84%, which is possibly due to relatively low MnBi content in these sample batches. This circumstance can be expected from the inhomogeneous MnBi formation which is varied by gravitational effect, initial mass, and other uncertain factors during LPS.

As seen in Figure 4.23(b), the value of M_s decreases noticeably from 45.31 to 2.38 emu/g or by 90.01% in the last condition. The H_{ci} rose from 5.98 kOe and saturated at the value of about 8.62 kOe after 48 hr heating time due to oxidation (M. Y. Sun et al., 2016). With a dramatic decrease of M_s, the $(BH)_{max}$ dropped sharply after heating where only $(BH)_{max}$ = 0.00004 MGOe were observed in the sample heated at 150 °C for 48 hr. The greatly reduction of ferromagnetic response in the heated sample is agreeable with a reduction of LTP-MnBi content shown in the XRD patterns of Figure 4.21(b). The reduction of MnBi content is considering much faster than by natural aging. It was reported that 54% drop of M_s for MnBi thin film with 10 nm Ta capping after 6 days of exposure time which was completely disappeared after 4 months (Villanueva et al., 2019). Another reports no significant change for MnBi thin film protected with a Ta capping layer while the sample without capping layer experiences a 35% drop after 14 days' exposure to air (J. Sun et al., 2016). In addition, it is reported that the magnetic properties of the MnBi powder which was sealed in epoxy resin and kept under Ar atmosphere showed no considerable change up to 80 days while the one kept under ambient atmosphere attributed to a dramatic decrease after exposing longer than 7 days (Ly et al., 2014). From above characterizations, it was found that thermal strongly affects to the magnetic

performance through the reduction of the MnBi content resulted from the segregation and oxide formation. This works pointed out that thermal is one of the crucial parameters for degradation, in addition to the atmosphere and protection.